Cytosolic MAPK signaling gates chloroplast protein import and photosynthetic capacity

Sarvesh Jonwal, Balakrishnan Rengasamy, Gopal Banerjee, Muskan Bansal, Mohit Mohit, Pallavi Sharma, and Alok Krishna Sinha*

National Institute of Plant Genome Research, New Delhi, 110067

*Corresponding author: Alok Krishna Sinha, Email: alok@nipgr.ac.in

Short title: MPK3-ACTPK1-RbcS modulates rice photosynthesis

Abstract

Chloroplast protein import is essential for photosynthesis, yet whether and how cytosolic signaling pathways dynamically regulate this process remains largely unknown. Here we uncover a signaling module that links mitogen activated protein kinase (MAPK) activity to fine tune the import of small subunit of Rubisco (RbcS) into the chloroplast. We show that MPK3 negatively regulates the cytosolic Raf-like kinase ACTPK1, which directly phosphorylates the transit peptide of RbcS precursor at Thr12. MPK3 directly phosphorylates ACTPK1, attenuating its kinase activity and thereby limiting RbcS transit peptide phosphorylation. Genetic and physiological analyses demonstrate that loss of MPK3 elevates ACTPK1 activity, increases RbcS phosphorylation and enhances Rubisco accumulation and CO_2 assimilation. On the other hand, ACTPK1 deficiency compromises these processes and photosynthetic performance. Phospho-mutant analyses further reveal that reversible phosphorylation of the RbcS transit peptide is required for efficient chloroplast import. Together, our findings establish chloroplast protein import as a signaling-regulated process and identify transit peptide phosphorylation a key check point integrating cytosolic MAPK signaling with photosynthetic capacity.

Introduction

Photosynthesis is the key photochemical process that drives the conversion of CO_2 and H_2O into organic carbon compounds. This process is regulated by multiple leaf traits, encompassing physiology, biochemistry, and development along with external environmental factors.

Photosynthetic proteins critical to this process are encoded by both the nuclear and chloroplast genomes. Chloroplast-encoded proteins are synthesized within the chloroplast, while nucleus-encoded chloroplastic proteins are transcribed in the nucleus, translated in the cytosol, and translocated to the chloroplast via a targeting signal peptide that directs them through the chloroplast membranes (Bruce, 2000; Jarvis & López-Juez, 2013). Once inside the chloroplast, these proteins are processed and assembled into functional complexes. Rubisco, a pivotal enzyme in CO_2 fixation, is a hexadecameric holoenzyme comprising eight large subunits (RbcL) and eight small subunits (RbcS). The translocation of the small subunit into the chloroplast is essential for holoenzyme assembly. In the cytosol, RbcS is synthesized as a precursor bearing an N-terminal transit peptide, stabilized by chaperones such as Hsp70 and targeted to the chloroplast, where it is processed, folded and assembled with RbcL by stromal chaperones and assembly factors including Cpn60/Cpn10 and RAF1 (Lee et al., 2009, 2013; Jarvis & López-Juez, 2013; Spreitzer, 2003; Feiz et al., 2012; Hauser et al., 2015). Efficient RbcS import is therefore required to stabilize the RbcL octamer and form functional Rubisco, and its failure severely compromises CO_2 fixation and photosynthetic performance (Andersson & Backlund, 2008).

Enhancing leaf photosynthesis is a major goal for improving crop productivity, and biochemical studies have identified multiple strategies to overcome intrinsic limitations of Rubisco and carbon assimilation (Long et al., 2006; Zhu et al., 2010; Gibson et al., 2011; Murchie & Niyogi, 2011; Covshoff & Hibberd, 2012; Ort et al., 2015; Simkin et al., 2019). Photosynthetic capacity is constrained by the catalytic properties of Rubisco, the efficiency of electron transport, RuBP regeneration, and developmental traits that influence light capture and CO_2 diffusion (von Caemmerer, 2000; Parry et al., 2007; Sharkey et al., 2007; Murchie & Lawson, 2013; Terashima et al., 2011; Mathan et al., 2016). While these biochemical and physiological determinants have been extensively characterized, the information about how regulatory signaling pathways control the targeting, stability and accumulation of photosynthetic proteins to coordinate photosynthetic performance is poorly understood (Evans, 2013).

Photosynthetic efficiency is further modulated by environmental fluctuations, such as light, temperature, and CO_2 concentration, which impact Rubisco activity, electron flow, and carbon assimilation (Kalaji et al., 2016; Sharma et al., 2020; Borba et al., 2023; Gao et al., 2024). To maintain optimal photosynthesis under these conditions, plants employ post-translational

modifications along with gene expression at transcriptional and translational levels, with phosphorylation playing a central role (Puthiyaveetil et al., 2009, 2010; Schönberg & Baginsky, 2012; Jonwal et al., 2021; Xiong D, 2024). Phosphorylation, mediated by kinases such as STN7, STN8, and cpCK2α, targets core photosystem proteins, light harvesting complexes, plastid transcription factors and Calvin cycle enzymes. They function by modulating their activity, stability, and interactions to balance electron flow, protect against photoinhibition, and optimize CO_2 fixation (Bellafiore et al., 2005; Reiland et al., 2009, 2011; Schönberg et al., 2017). While phosphorylation is a well-established mechanism in photosynthetic regulation, the role of Mitogen-Activated Protein Kinase (MAPK) cascades in this context remains underexplored.

MAPK cascades are conserved signalling pathways in eukaryotes. They operate in three tiers: MAPKKKs activate MAPKKs at a conserved S/T-X5-S/T motif, which in turn activate MAPKs at the TE/DY motif (Hamel et al., 2006). This hierarchical cascade ensures precise signal transmission, with MAPKKKs as initiators, MAPKKs as intermediates, and MAPKs as terminal effectors that phosphorylate substrates to regulate cellular responses (Rodriguez et al., 2010). MAPKs regulates growth, development, immunity, and defense in response to environmental and endogenous cues (Sinha et al., 2011; Manna et al., 2023). Evidence from multiple plant systems highlights MAPKs as important regulators of photosynthesis. In *Nicotiana attenuata* and *Arabidopsis*, MPK4 influences stomatal conductance, thylakoid organization, and PSII efficiency, thereby affecting carbon assimilation and energy distribution (Hettenhausen et al., 2012; Gawronski et al., 2014; Witoń et al., 2016, 2021). Moreover, *StMPK3*, *StMPK11*, and *PeMPK7*, modulate photosynthetic gene expression and stomatal dynamics under stress (Zhu et al., 2020, 2021; Gao et al., 2024). Furthermore, MPK4, MPK12, regulate CO_2-induced stomatal behaviour through Raf-like MAPKKK *HT1* (Hashimoto et al., 2016; Hiyama et al., 2017; K. Tõldsepp et al., 2018; Takahashi et al., 2022). MPK3 and MPK6 are rapidly activated during stress and immunity and often correlate with reduced photosynthetic activity (Su et al., 2018). Consistent with this, MPK3 overexpression has been shown to strongly reduce photosynthetic performance, whereas MPK6 exerts a modest positive effect, highlighting their distinct roles even under non-stressful conditions (Jonwal et al., 2023). However, the precise molecular mechanisms by which MAPKs influence photosynthesis remain poorly understood.

Here, we uncover a signaling framework that connects cytosolic MAPK activity to the photosynthetic capacity. We demonstrated that MPK3 modulates the activity of the Raf-like kinase ACTPK1, a cytosolic serine/threonine kinase previously implicated in nutrient signaling through its regulation of ammonium transporters (Beier et al., 2018). Notably, Arabidopsis homologues of ACTPK1 (STY8, STY17 and STY46) have been associated with chloroplast protein targeting and photosynthetic function (Lamberti et al., 2011), suggesting a broader role for this kinase family in organelle biogenesis. Building on these observations, our findings position ACTPK1 at the interface of MAPK signaling and chloroplast protein import. We show that MPK3 constrains ACTPK1 activity, thereby influencing the stability and targeting efficiency of the Rubisco small subunit precursor (RbcS). Our results further indicate that phosphorylation of the RbcS transit peptide operates as a reversible regulatory switch rather than a static modification, revealing a dynamic control mechanism that coordinates cytosolic signaling inputs with chloroplast protein import and photosynthetic output in rice

Results

MPK3 negatively regulates photosynthetic Carbon Assimilation

Overexpression of *MPK3* has been reported to adversely affects photosynthetic performance in rice (Jonwal et al., 2023). To dissect the molecular mechanism underlying this observation, we analyzed the photosynthesis and related parameters in two independent *MPK3* knockout lines (*mpk3 ko1* and *mpk3 ko2*) and two dexamethasone (DEX)-inducible *MPK3* overexpression lines (*MPK3-23* and *MPK3-24*) under ambient growth conditions (Banerjee et al., 2025; Singh et al., 2019). Photosynthetic pigments (chlorophyll a, chlorophyll b, and carotenoids) essential for light absorption and photoprotection were significantly higher in *mpk3 ko* and reduced in *MPK3 OE* lines compared to WT (Supplemental Fig. S1A-D). Elevated levels in knockout lines likely enhance light-harvesting efficiency and overall photosynthetic capacity, while reduced levels in overexpression lines may impair these processes. Consistently, net CO_2 assimilation rates (*A*) were significantly higher in *mpk3 ko* lines and lower in *MPK3 OE* lines than in WT (Fig. 1A). Under ambient CO_2 (400 µmol mol^{-1}), *A* reached 29.78 and 30.48 µmol m^{-2} s^{-1} in *mpk3 ko1* and *ko2* (18–21% higher than WT), whereas *MPK3 OE* lines showed only 17.75 and 17.67 µmol m^{-2} s^{-1} (~29% lower than WT; Table 1).

Photosynthetic efficiency is determined by CO_2 diffusion into the chloroplast stroma (stomatal conductance, gs) and subsequent carboxylation (Evans, 2021). To explore the basis for the

125 observed differences in *A*, we measured *gs* and intercellular CO_2 concentration (*Ci*). Notably,
126 *mpk3 ko* plants with higher *A* exhibited elevated *gs* whereas *MPK3 OE* plants showed reduced
127 *gs* compared to WT. However, C_i values remained comparable across genotypes (Fig. 1B and
128 Supplemental Fig. S1E), indicating that the altered photosynthetic rates stem primarily from
129 differences in carboxylation efficiency rather than CO_2 availability.

130 Since *mpk3 ko* plants showed higher *A* and *gs*, but unchanged *Ci*, we used *A/Ci* and *A/Q* curve
131 analyses to distinguish the effects of MPK3 on CO_2 fixation versus light-dependent processes
132 (Farquhar et al., 1980; Long & Bernacchi, 2003). With increasing CO_2, *mpk3 ko* plants
133 exhibited consistently higher *A* compared to WT, with a CO_2-saturated maximum assimilation
134 rate (*Amax*) of 41.31 ± 0.68 µmol CO_2 m^{-2} s^{-1} (~14% higher than WT), while *MPK3 OE* lines
135 showed a reduced *Amax* of 27.55 ± 1.45 µmol CO_2 m^{-2} s^{-1} (~31% lower than WT) (Fig. 1C
136 and Table 1). In contrast, light-response curves were similar among genotypes, with
137 comparable light-saturated assimilation rates (Fig. 1D), indicating that MPK3 primarily
138 modulates CO_2-responsive processes, such as Calvin cycle efficiency, rather than light-
139 dependent reactions.

140 Consistent with the preferential effect of MPK3 on CO_2-responsive photosynthesis, Farquhar-
141 von Caemmerer-Berry (FvCB) modelling of the *A/Ci* curves revealed that *Vcmax*, *J*, and *TPU*
142 were significantly enhanced in *mpk3 ko* plants but markedly reduced in *MPK3 OE* lines relative
143 to WT (Fig. 1E, F & G), indicating that MPK3 negatively regulates the biochemical capacity
144 for CO_2 fixation and regeneration in the Calvin cycle. These results establish *MPK3* as a
145 negative regulator of photosynthetic efficiency, as knockout lines exhibited enhanced pigment
146 accumulation, stomatal conductance, and carboxylation efficiency, boosting photosynthesis,
147 while overexpression lines showing the opposite trend.

148 **MPK3 Regulates Rubisco Activity via RbcS Phosphorylation**

149 Carboxylation efficiency is primarily governed by Rubisco activity and the availability of its
150 substrate RuBP (Farquhar et al., 1980). Supporting the higher *Vcmax* in *mpk3 ko* plants, both
151 RuBP utilisation and Rubisco activity were significantly increased compared with WT (Fig.
152 1H, I). The observation indicate that MPK3 adversely affect Rubisco function and RuBP
153 regeneration, thereby limits carboxylation efficiency. The fact that Rubisco activity depends
154 on the assembly of the nuclear-encoded small subunit (RbcS) with the chloroplast-encoded
155 large subunit (RbcL), and that MPK3 localises predominantly to the nucleus and cytosol

156 (Supplemental Fig. S2A, B), we hypothesised that MPK3 regulates Rubisco function via
157 transcriptional or post-translational control of RbcS rather than through direct effects on
158 chloroplast-resident RbcL.

159 Accordingly, to test whether MPK3 regulates RbcS post-translationally, we examined RbcS
160 phosphorylation by Phos-tag analysis and detected an upshift of RbcS band indicative of
161 phosphorylation in both WT and *mpk3 ko* plants. Notably, the phosphorylated RbcS band was
162 consistently more intense in *mpk3 ko* plants compared to WT, suggesting enhanced RbcS
163 phosphorylation in the absence of *MPK3* (Fig. 1J). This higher RbcS phosphorylation in *mpk3*
164 *ko* is positively correlated with higher Rubisco activity and carboxylation rates.

165 These findings imply that MPK3 does not directly phosphorylate RbcS but rather suppresses
166 the activity of another kinase responsible for this modification. In *mpk3 ko* plants, where MPK3
167 is absent, this another "missing" kinase remains active, leading to increased RbcS
168 phosphorylation. Given the functional overlap between MPK3 and MPK6, we tested whether
169 MPK6 could act as this "missing" kinase. However, yeast two-hybrid (Y2H) and *in vitro* kinase
170 assays revealed no interaction or phosphorylation of RbcS by either MPK3 or MPK6
171 (Supplemental Fig. S2C & D), ruling out MPK6 as the "missing" kinase. These findings
172 strongly suggest that MPK3 indirectly modulates Rubisco activity by regulating RbcS
173 phosphorylation via an unidentified kinase.

174 **ACTPK1 may act as a Candidate "missing" Kinase in MPK3-RbcS module**

175 To identify the kinase responsible for elevated RbcS phosphorylation in *mpk3 ko* plants, we
176 conducted a literature survey focusing on known kinases that modify RbcS or its precursor. In
177 *Arabidopsis*, the RbcS transit peptide is phosphorylated by the cytosolic STY kinases, STY8,
178 STY17 and STY46, which regulate chloroplast import and thereby influence Rubisco assembly
179 and photosynthetic performance (Lamberti et al., 2011). A homology search using AtSTY46
180 identified a rice ACT-domain–containing kinase, ACTPK1 (LOC_Os02g02780)
181 (Supplemental Fig. S3A), which clusters within the Group-C Raf-like MAPKKKs and shows
182 strong sequence similarity to STY8, STY17 and STY46 (Supplemental Fig. S3B, C) (Beier et
183 al 2018; Rao et al., 2010). Notably, ACTPK1 contains multiple canonical S/TP motifs
184 corresponding to MAPK phosphorylation sites (Supplemental Fig. S3D), suggesting potential
185 regulation by MPK3. Given these structural and sequence similarities, ACTPK1 emerges as a
186 strong candidate for the kinase suppressed by MPK3 in regulating RbcS phosphorylation.

187 **MPK3 physically interacts with ACTPK1**

188 To test whether ACTPK1 is regulated by MPK3, we first examined their physical interaction,
189 as MAPKs typically regulate downstream targets through direct binding and phosphorylation
190 (Manna et al., 2023). We initially assessed the interaction between ACTPK1 and MPK3 in
191 yeast cell (*Saccharomyces cerevisiae*) using Y2H assay. ACTPK1 fused to the GAL4 DNA-
192 binding domain (BD) and MPK3 fused to the GAL4 activation domain (AD), were co-
193 transformed into the Y2H Gold strain in different combinations. Y2H assay showed that
194 ACTPK1 physically interacted with MPK3 (Fig. 2A), with the p53–T7 pair and empty-vector
195 combinations serving as positive and negative controls, respectively.

196 The interaction was confirmed *in planta* by bimolecular fluorescence complementation (BiFC)
197 assay in *Nicotiana benthamiana.* ACTPK1 was fused to the N-terminal half of enhanced yellow
198 fluorescent protein (nYFP), while MPK3 was fused to the C-terminal half (cYFP). Strong YFP
199 fluorescence was detected in *N. benthamiana* cells co-expressing ACTPK1–nYFP and MPK3–
200 cYFP, but not in control combinations, including ACTPK1 with MPK6 (Fig. 2B). The
201 association was further validated by co-immunoprecipitation of ACTPK1–Flag with MPK3–
202 GFP from *N. benthamiana* extracts, whereas no signal was detected in control samples (Fig.
203 2C). These results establish a specific physical interaction between MPK3 and ACTPK1,
204 prompting us to examine whether MPK3 functionally regulates ACTPK1 by phosphorylation.

205 **MPK3 phosphorylates ACTPK1 and supress its kinase activity**

206 As a putative Raf like MAPKKK, ACTPK1 was predicted to exhibit kinase activity. To test
207 this possibility, the coding sequence of ACTPK1 was fused with glutathione S-transferase
208 (GST) for protein purification. The resultant purified protein was subjected to *in vitro* kinase
209 assay with myelin basic protein (MBP), a widely used universal kinase substrate (Eichberg and
210 Iyer, 1996). Briefly, GST-ACTPK1 was incubated with MBP in kinase assay buffer
211 supplemented with λ^{32}P-ATP for 30 min at 30°C and the reaction products were resolved by
212 SDS-PAGE. Autoradiography revealed strong phosphorylation signals corresponding to both
213 ACTPK1 and MBP, indicating that ACTPK1 possesses both auto- and trans-phosphorylation
214 activities (Supplemental Fig. S4A).

215 To test whether ACTPK1 is a direct substrate of MPK3, we generated catalytically inactive
216 variants of ACTPK1 to eliminate background phosphorylation arising from its intrinsic kinase

217 activity. To generate a catalytically inactive ACTPK1 variant, a conserved lysine in the
218 predicted catalytic subdomain II (K332), identified by sequence alignment with homologues
219 (Supplemental Fig. S4B), was mutated to arginine (ACTPK1^{K332R}) by site-directed
220 mutagenesis (Supplemental Fig. S4C). This mutation abolished MBP trans-phosphorylation
221 while retaining ACTPK1 autophosphorylation (Supplemental Fig. S4A), indicating that K332
222 is required for trans-phosphorylation but not for autophosphorylation. To further eliminate
223 residual autophosphorylation, a second conserved lysine in subdomain VI (K428) was mutated
224 in the K332R background (ACTPK1^{K332R,K428R}) (Supplemental Fig. S4D), which abolished
225 both auto- and trans-phosphorylation (Supplemental Fig. S4A), generating a fully inactive
226 ACTPK1 variant.

227 Using this kinase-dead ACTPK1^{K332R,K428R} protein as substrate for MPK3, an in-solution kinase
228 assays demonstrated that MPK3 directly phosphorylates ACTPK1 (Fig. 2D), whereas GST
229 alone was not phosphorylated, confirming the specificity of the reaction. In *Medicago sativa*,
230 OMTK1 **(**a MAPKKK**)** was shown to directly phosphorylate and activate the MMK3 (a
231 MAPK**)**, bypassing the canonical MAPKK step (Nakagami et al., 2004). This represents a rare
232 exception to the typical three-tier MAPK cascade and highlights alternative signalling modes
233 in plants. Since the evidence of reverse signalling in MAPK modules is rare, we tested whether
234 ACTPK1 could phosphorylate MPK3. However, ACTPK1 failed to phosphorylate a kinase-
235 dead MPK3 variant (MPK3^{K65R}) (Supplemental Fig. S4E), indicating that phosphorylation
236 occurs unidirectionally from MPK3 to ACTPK1.

237 To assess the functional consequence of MPK3-mediated phosphorylation of ACTPK1, we
238 immunoprecipitated ACTPK1 from WT and *mpk3 ko* plants and measured its kinase activity
239 using MBP as substrate. ACTPK1 immunocomplexes from *mpk3 ko* plants displayed
240 substantially higher kinase activity than those from WT (Fig. 2E), demonstrating that MPK3
241 negatively regulates ACTPK1 kinase activity, likely through direct phosphorylation-mediated
242 inhibition.

243 **ACTPK1 interacts with and phosphorylates RbcS at its signal peptide**

244 To establish ACTPK1 as the kinase responsible for RbcS phosphorylation in our pathway, we
245 analysed *RbcS3*, the most abundant *RbcS* isoform in rice (~50% of the total RbcS pool; Suzuki
246 et al., 2007). Since ACTPK1 is a cytosolic kinase, we reasoned that its interaction with RbcS
247 would occur in the cytoplasm prior to plastid import and therefore used the precursor form of

248 RbcS for all interaction assays. Y2H analysis revealed a direct interaction between ACTPK1
249 and precursor RbcS (Fig. 3A). This interaction was further confirmed *in planta* by BiFC assay
250 in *N. benthamiana*, where a strong YFP signal was detected in the cells co-expressing
251 ACTPK1–nYFP and RbcS–cYFP (Fig. 3B), demonstrating that ACTPK1 physically associates
252 with RbcS *in vivo*.

253 We next tested whether this interaction results in phosphorylation of RbcS. *In vitro* kinase
254 assays using bacterially expressed GST-ACTPK1 and GST-RbcS showed robust
255 phosphorylation, demonstrating that ACTPK1 directly phosphorylates RbcS (Fig. 3C). To
256 pinpoint the region of phosphorylation, we cloned and expressed precursor RbcS (containing
257 the signal peptide) and its mature form lacking the signal peptide (mRbcS). *In vitro* kinase
258 assay revealed that phosphorylation occurred exclusively on the precursor but was abolished
259 in mRbcS, indicating that the phosphorylation site resides within the signal peptide
260 (Supplemental Fig. S5A,B). *In silico* analysis using NetPhos3.1 identified three high-
261 confidence candidate phosphosites within the signal peptide (Thr12, Ser31 and Ser34;
262 Supplemental Fig. S5C). Alanine-substitution mutants ($RbcS^{S31A}$, $RbcS^{S34A}$ and $RbcS^{T12A}$)
263 were generated in precursor RbcS form and subsequently tested in kinase assays (Supplemental
264 Fig. S5D). Phosphorylation was retained in $RbcS^{S31A}$ and $RbcS^{S34A}$ but completely abolished
265 in $RbcS^{T12A}$ (Fig. 3D; Supplemental Fig. S5E).

266 Together, these findings demonstrate that ACTPK1 directly phosphorylates RbcS at Thr12
267 within its signal peptide. This modification likely act as a regulatory checkpoint in the
268 cytoplasm, modulating RbcS import into chloroplasts and thereby fine-tuning Rubisco
269 assembly and function.

270 **Phosphorylation by ACTPK1 regulates RbcS stability and chloroplast targeting**
271 **competence**

272 Since ACTPK1 phosphorylates RbcS at Thr12 within its chloroplast transit peptide, a region
273 essential for TOC/TIC-mediated targeting, we tested whether modification of this residue
274 affects RbcS chloroplast import. To this end, phospho-dead ($RbcS^{T12A}$) and phospho-mimetic
275 ($RbcS^{T12D}$) variants of the RbcS precursor were generated by site directed mutagenesis using
276 overlapping PCR (Fig. 4A). The mutant versions along with Wild-type were fused to C-
277 terminal GFP and transiently expressed in rice protoplasts derived from WT, *mpk3 ko*, and
278 *actpk1 ko* backgrounds.

279 Wild-type RbcS–GFP predominantly localized to chloroplasts, whereas both the phospho-dead
280 ($RbcS^{T12A}$) and phospho-mimetic ($RbcS^{T12D}$) variants displayed markedly reduced chloroplast
281 accumulation and instead localized primarily to the cytosol and perichloroplast regions (Fig.
282 4B). Notably, the phospho-dead $RbcS^{T12A}$ variant accumulated in distinct cytosolic puncta,
283 suggesting aggregation of precursor protein, whereas the phospho-mimetic $RbcS^{T12D}$ variant
284 remained diffusely distributed in the cytosol but still failed to efficiently localize to
285 chloroplasts. These observations suggest that phosphorylation of Thr12 may help maintain the
286 RbcS precursor in a soluble, import-competent state, while subsequent dephosphorylation may
287 be required for productive chloroplast import. The impaired targeting of both phospho-dead
288 and phospho-mimetic variants therefore indicates that efficient chloroplast import does not
289 depend on a fixed phosphorylation state but requires regulated phosphorylation dynamics.
290 Supporting this interpretation, pharmacological inhibition of protein dephosphorylation by
291 okadaic acid results in reduced chloroplast accumulation of wild-type RbcS–GFP,
292 phenocopying the localization defect observed for the phospho-mimetic variant (Fig. 4C).
293 Moreover, the ability of the phospho-dead and phospho-mimetic mutant to partly localize to
294 chloroplasts indicates that phosphorylation is not strictly required for import. However, its
295 reduced efficiency compared to the wild-type RbcS suggests that dynamic phosphorylation–
296 dephosphorylation, rather than a constitutive state, optimizes chloroplast targeting. Similar
297 localization pattern was observed in *mpk3 ko* protoplasts (Supplemental Fig. S6A).

298 Strikingly, no detectable GFP signal from RbcS–GFP was observed in *actpk1 ko* protoplasts,
299 despite multiple independent transfection attempts (Supplemental Fig. S6B). In line with this
300 observation, stable transgenic lines expressing RbcS–GFP showed robust chloroplast
301 localization in the WT background but no detectable signal in the *actpk1 ko* background (Fig.
302 4D). Treatment with the proteasome inhibitor MG132 did not restore GFP accumulation,
303 indicating that proteasome-dependent degradation alone does not fully account for the loss of
304 RbcS–GFP signal (Supplemental Fig. S6B).

305 To directly examine the RbcS stability, we performed a cell-free protein degradation assay by
306 incubating bacterially expressed RbcS protein with crude extracts from WT, *ACTPK1 OE* and
307 *actpk1 ko* plants. RbcS was rapidly destabilized in extracts derived from *actpk1 ko* plants,
308 whereas it remained comparatively stable in WT and *ACTPK1 OE* extracts (Fig. 4E). These
309 results indicate that ACTPK1 activity contributes to maintaining RbcS protein stability.

310 To further substantiate these observations, quantitative RT-PCR analysis revealed reduced
311 RbcS transcript levels in *actpk1 ko* plants compared with WT and *ACTPK1 OE* lines (Fig. 4F),
312 suggesting that ACTPK1 influences RbcS accumulation at multiple regulatory levels.
313 Together, these findings demonstrate that ACTPK1-dependent phosphorylation is required to
314 maintain RbcS stability and chloroplast targeting competence, thereby supporting efficient
315 precursor accumulation and import.

316 **ACTPK1 positively regulates photosynthesis**

317 To further validate this pathway and its impact on photosynthesis, we generated *ACTPK1*
318 overexpression (*OE*) and knockout (*ko*) lines, along with *MPK3-ACTPK1* double knockout
319 (*mpk3actpk1 ko*) *in the* japonica rice cultivar Taipae309. Three independent *OE* lines (*ACTPK1*
320 *OE19*, *ACTPK1 OE24* and *ACTPK1 OE33*) with the highest transcript accumulation were
321 selected for detailed analysis (Supplemental Fig. S7A, B & C). *actpk1 ko* lines were generated
322 via CRISPR/Cas9-mediated genome editing technology and three independent *actpk1* mutant
323 alleles, *actpk1 ko12 (*deletion of four nucleotides*), actpk1 ko14* (single nucleotide insertion)
324 and *actpk1 ko19* (single nucleotide insertion), were selected for detailed analysis
325 (Supplemental Fig. S7D & E). The double knockout was generated by mutating ACTPK1 in
326 *mpk3 ko* background using CRISPR-Cas9 genome editing tool. A mutant line harbouring a
327 single-nucleotide insertion in the ACTPK1 coding sequence was selected for further analysis
328 (Supplemental Fig. S7F).

329 To study the impact of ACTPK1 on photosynthesis we measured gas-exchange parameters in
330 the flag leaf of *ACTPK1 OE* and *actpk1 ko* lines at heading stage using LI-COR 6800 system,
331 targeting a 2 cm^2 area from 9:00 am to 11:00 am. At ambient CO_2 concentration, the mean *A*
332 of *actpk1 ko* plants were significantly lower that WT and *ACTPK1 OE* lines, with *actpk1 ko*
333 showing 12.973 ± 0.99 μmol m^{-2} s^{-1}, a 36–45% decrease compared to WT and *ACTPK1 OE*
334 plants (Fig. 5A & Table 2). In contrast, mean *A* in *ACTPK1 OE* lines were comparable to WT,
335 indicating that overexpression does not disturb the kinase's functional balance.

336 Photosynthesis is positively corelated with stomatal conductance. Stomatal conductance
337 mirrored these patterns, with *actpk1 ko* lines showing lower values supporting the reduced
338 photosynthetic capacity (Fig. 5B). *Ci* remained unchanged among genotypes, ruling out CO_2
339 availability as the cause of reduced photosynthesis in *actpk1 ko* plants. (Supplemental Fig. 8).

340 Moreover, *A/Ci* response curves revealed a pronounced reduction in net photosynthetic rate in
341 *actpk1 ko* lines compared to WT and *ACTPK1 OE* lines across all tested CO_2 concentrations
342 (Fig. 5C). Interestingly, *ACTPK1 OE* lines exhibited photosynthetic rates comparable to WT
343 across all tested CO_2 concentrations. *A/Q* curves further showed that *actpk1 ko* lines had
344 diminished light-saturated photosynthesis, while *ACTPK1 OE* lines sustained slightly higher
345 rates relative to WT (Fig. 5D).

346 Modelling of the *A/Ci* curves provided further insight into the biochemical basis of this decline.
347 The CO_2-saturated photosynthetic capacity (A_{max}) was reduced by ~31–37% in *actpk1 ko* plants
348 (26.2 ± 0.5 µmol m^{-2} s^{-1}) compared with WT (39.3 ± 0.8 µmol m^{-2} s^{-1}) and *OE* lines (39.9 ±
349 1.5 µmol m^{-2} s^{-1}) (Table 2). Moreover, *actpk1 ko* lines displayed significantly reduced values
350 for *Vcmax*, *J*, and *TPU* (Fig. 5E, F & G). These reductions strongly suggest impaired Rubisco
351 activity and compromised electron transport in *actpk1 ko* plants. Collectively, these findings
352 demonstrate that the absence of ACTPK1 leads to a substantial loss in Rubisco-dependent
353 photosynthetic capacity.

354 **MPK3-ACTPK1 operate in a linear signaling cascade to regulate photosynthesis**

355 Next, we analysed the photosynthetic phenotypes of *mpk3*, *actpk1*, and *mpk3actpk1* mutants.
356 *A/Ci* response curves revealed a marked increase in net CO_2 assimilation in *mpk3 ko* plants,
357 with a steep rise and elevated plateau, whereas *actpk1 ko* lines displayed strongly reduced
358 photosynthetic rates relative to WT, across a range of intercellular CO_2 concentrations (Fig.
359 6A). Crucially, the *mpk3actpk1* double mutant mirrors the *actpk1 ko* phenotype, with low
360 assimilation rate, rather than the enhanced *mpk3* ko mutant. This suppression in the
361 *mpk3actpk1* double mutant indicates that ACTPK1 works downstream of MPK3 as in absence
362 of ACTPK1, knocking out MPK3 cannot rescue the pathway. A *s*imilar trend was observed for
363 light response (*A/Q*) curves where *mpk3 ko* plants maintained slightly elevated photosynthetic
364 rates under increasing irradiance, while *actpk1 ko* and *mpk3actpk1 ko* lines exhibited impaired
365 light-saturated photosynthesis (Fig. 6B).

366 Moreover, the biochemical insights support the above observations. *Vcmax* was highest in
367 *mpk3 ko* lines but drops to *actpk1 ko* levels in and *mpk3actpk1 ko* plants. *J* and *TPU* followed
368 the same trend, enhanced in *mpk3 ko*, and reduced in *actpk1 ko* and *mpk3actpk1 ko* plants
369 compared to WT. (Fig. 6C, D & E). Rubisco activity measurements further confirmed this

370 trend, with higher activity in *mpk3 ko* and strongly diminished activity in *actpk1 ko* and
371 *mpk3actpk1 ko* (Fig. 6F, G).

372 Confirming the observation of the altered carboxylation capacity, BN-PAGE and immunoblot
373 analyses revealed that Rubisco holoenzyme abundance, as well as RbcS protein levels, were
374 increased in *mpk3 ko* plants and reduced in *MPK3 OE* lines compared with WT (Fig. 6H).
375 Conversely, *actpk1 ko* plants showed reduced Rubisco holoenzyme abundance together with
376 decreased RbcS levels, whereas *ACTPK1 OE* plants accumulated higher amounts of Rubisco
377 and RbcS relative to WT (Fig. 6I). These changes in Rubisco accumulation mirror the
378 corresponding alterations in photosynthetic capacity across the MPK3 and ACTPK1 genetic
379 backgrounds.

380 The finding that *mpk3actpk1* double mutants phenocopy the *actpk1 ko* mutants, rather than
381 *mpk3 ko* alone, indicates that ACTPK1 acts genetically downstream of MPK3. Moreover, the
382 loss of the enhanced photosynthetic performance observed in *mpk3 ko* plants upon ACTPK1
383 disruption highlights a linear regulatory hierarchical, in which MPK3 negatively regulates
384 photosynthesis by suppressing ACTPK1 activity.

385 To directly link the genetic hierarchy to RbcS regulation, we examined RbcS phosphorylation
386 across these genotypes using Phos-tag SDS–PAGE. Phos-tag analysis revealed a distinct
387 mobility shift of RbcS in WT and *ACTPK1 OE* seedlings, indicative of phosphorylation. In
388 contrast, no shift was detected in *actpk1 ko* or *mpk3actpk1 ko* seedlings, demonstrating that
389 enhanced RbcS phosphorylation in *mpk3 ko* plants is due to the presence of ACTPK1, thus
390 placing ACTPK1 downstream in this cascade (Fig. 6J). This hierarchy aligns with our
391 biochemical evidence that MPK3 phosphorylates ACTPK1 thereby inhibiting its kinase
392 activity and preventing ACTPK1-mediated phosphorylation of RbcS.

393 **ACTPK1 positively regulates plant biomass and yield**

394 Photosynthetic efficiency directly influences plant productivity, where enhanced carbon
395 assimilation supports plant growth and biomass. We next examined the effect of ACTPK1-
396 mediated photosynthesis regulation on plant growth and development. *ACTPK1 OE* and WT
397 seedlings exhibited enhanced shoot and root length compared to *actpk1 ko* which displayed
398 retarded growth, indicating robust vegetative growth fueled by increased carbon fixation
399 (Supplemental Fig. S9A-C). At maturity, plant height, tiller number per plant, and plant

400 biomass were significantly reduced in *actpk1 ko* lines relative to *ACTPK1 OE* and WT (Fig.
401 7A-D). Moreover, striking differences were observed in flag leaf angle, *ACTPK1 OE* plants
402 displayed highly erect flag leaves with narrow angles (8°–19°), WT plants had moderately open
403 leaves (14°–29°), whereas *actpk1 ko* lines exhibited leaves with widest angles (45°–75°)
404 (Supplemental Fig. S9D-E). As leaf angle strongly influences light interception, these
405 differences likely have direct consequences for photosynthetic efficiency. Furthermore,
406 flowering time was markedly delayed in *actpk1 ko* by 10–15 days compared to *ACTPK1 OE*
407 and WT. While WT and *ACTPK1 OE* lines-initiated flowering at 80–85 days, *actpk1 ko* plants
408 flowered at approximately 100–105 days after sowing, indicating a potential regulatory role of
409 ACTPK1 in floral transition (Supplemental Fig. S9F). These data suggest that absence of
410 *ACTPK1* disrupts developmental timing and architecture, likely due to impaired photosynthesis
411 and resource allocation.

412 Interestingly, *ACTPK1* also affects seed architecture and yield. *actpk1 ko* plants exhibited
413 significantly lower number of panicles per plant compared to *ACTPK1 OE* and WT (Fig. 7E).
414 Lower panicle number resulted in reduced grain yield per plant in *actpk1 ko* plants (Fig. 7F).
415 Interestingly, seeds from *actpk1 ko* plants were not only longer but also wider than those from
416 WT and *ACTPK1* OE lines, resulting in a significantly higher 100-seed weight (Fig. 7G,
417 Supplemental Fig. S9G-I). However, these advantages in seed productivity were offset by a
418 substantial reduction in tiller number and panicle number, traits that are key contributors to
419 overall yield. Thus, while *ACTPK1* knockout promotes the formation of larger and heavier
420 seeds, it concurrently suppresses the production of structures such as tillers and panicles that
421 bears reproductive organs, highlighting its role in balancing the trade-off between seed size
422 and seed number.

423 **Discussion**

424 Chloroplast protein import must be tightly coordinated with cytosolic signalling to sustain
425 photosynthetic performance. Although phosphorylation of chloroplast transit peptides has been
426 proposed to influence precursor targeting for more than two decades, the physiological
427 relevance and regulatory logic of this modification have remained unresolved. Here, we
428 identify a MAPK-regulated signalling module in rice in which MPK3 modulates the activity
429 of the cytosolic Raf-like kinase, ACTPK1 to dynamically regulate the phosphorylation status
430 of the RbcS precursor. Our results demonstrate that neither constitutive phosphorylation nor
431 permanent loss of phosphorylation is sufficient for efficient RbcS import, indicating that

432 reversible phosphorylation rather than a fixed phosphorylation state underpins productive
433 chloroplast translocation. This dynamic regulatory model reconciles earlier biochemical
434 observations with *in vivo* import behaviour and provides a mechanistic framework through
435 which cytosolic signalling pathways can fine-tune chloroplast protein targeting and
436 photosynthetic capacity.

437 The central mechanistic finding of this study is that MPK3 negatively regulates ACTPK1,
438 which directly phosphorylates the RbcS precursor at Thr12 within its transit peptide. Genetic
439 and biochemical analyses demonstrate that MPK3 suppresses ACTPK1 activity, thereby
440 modulating RbcS phosphorylation, Rubisco accumulation and photosynthetic capacity.

441 Phosphorylation has long been implicated in chloroplast protein import, particularly through
442 modification of transit peptides that modulate precursor handling and targeting. In Arabidopsis,
443 the STY kinases STY8, STY17 and STY46 phosphorylate RbcS transit peptides and influence
444 chloroplast protein import (Lamberti et al., 2011). Our identification of ACTPK1 as the
445 functional rice homolog of this kinase family places RbcS transit-peptide phosphorylation
446 within a genetically defined MPK3-regulated signaling pathway.

447 MPK3, localized in the cytoplasm and nucleus, indirectly regulates photosynthesis by
448 modulating RbcS phosphorylation dynamics through ACTPK1. Protein phosphorylation is a
449 well-established regulator of photosynthesis, coordinating light harvesting, energy distribution
450 and photoprotection (Tikkanen and Aro, 2012; Rochaix, 2014), and contributes to chloroplast
451 protein import by modifying transit peptides and translocon components (Waegemann and
452 Soll, 1996; May and Soll, 2000; Jarvis and Robinson, 2004). Rubisco subunits themselves are
453 known phosphoproteins, and these modifications can influence enzyme stability and function
454 (Houtz et al., 1989; Grabsztunowicz et al., 2017). In accordance with this regulatory
455 framework, we show that RbcS phosphorylation is enhanced in *mpk3 ko* plants and is
456 associated with increased Rubisco accumulation and elevated carboxylation efficiency.
457 Mechanistically, ACTPK1 directly phosphorylates the RbcS precursor, thereby providing the
458 molecular basis through which MPK3 signaling regulates chloroplast protein targeting.

459 MPK3 directly phosphorylates ACTPK1, providing a mechanistic basis for its negative
460 regulation and establishing a non-canonical MAPK module linking cytosolic signalling to
461 chloroplast protein targeting. Protein–protein interaction assays, including Y2H, BiFC and Co-
462 IP, demonstrate direct association between MPK3 and ACTPK1, while *in vitro* kinase assays

463 establish unidirectional phosphorylation of ACTPK1 by MPK3. Functional analyses further
464 show that ACTPK1 kinase activity is enhanced in *mpk3 ko* plants, demonstrating that MPK3-
465 mediated phosphorylation negatively regulates ACTPK1 activity. This kinase-on-kinase
466 regulation explains how MPK3 modulates RbcS phosphorylation, Rubisco accumulation and
467 photosynthetic performance.

468 ACTPK1 loss also causes pleiotropic developmental and yield-related phenotypes, including
469 delayed flowering, reduced tillering and altered leaf architecture, which correlate with reduced
470 CO_2 assimilation and carboxylation efficiency. These findings indicate that ACTPK1 activity
471 is required to sustain photosynthetic capacity and normal plant productivity. Given the
472 established role of ACTPK1 in ammonium transporter regulation (Beier et al., 2018; Shilpha
473 et al., 2023), these phenotypes likely reflect combined effects of impaired photosynthesis and
474 altered metabolic homeostasis rather than a direct developmental signaling function of the
475 MPK3–ACTPK1–RbcS module.

476 At the molecular level, ACTPK1 phosphorylates RbcS at Thr12 within its transit peptide, as
477 demonstrated by *in vitro* kinase assays and site-directed mutagenesis. This modification
478 contributes to maintaining RbcS in an import-competent cytosolic state. On the other hand our
479 phosphomutant and inhibitor analyses indicate that reversible phosphorylation, finely
480 coordinating kinase and phosphatase activities, is necessary to support efficient chloroplast
481 translocation. In accordance with this model, the phosphomimetic $RbcS^{T12D}$ variant and
482 phospho-dead $RbcS^{T12A}$ variant shows reduced chloroplast targeting, in agreement with
483 previous studies demonstrating the importance of transit peptide phosphorylation dynamics for
484 precursor handling and import (Waegemann and Soll, 1996; May and Soll, 2000; Lee et al.,
485 2009; Jarvis & López-Juez, 2013). These observations indicate that phosphorylation is not
486 simply required or inhibitory for import, but rather that regulated phosphorylation dynamics
487 are necessary to maintain precursor competence for chloroplast targeting. Transit peptide
488 phosphorylation has been proposed to regulate precursor interaction with cytosolic chaperones
489 such as 14-3-3 proteins and Hsp70, which maintain precursors in an import-competent state,
490 suggesting that ACTPK1-mediated phosphorylation may regulate RbcS through similar
491 mechanisms.

492 The absence of detectable RbcS–GFP signal in *actpk1* mutant cells, together with its rapid
493 destabilization in degradation assays, suggests that ACTPK1 activity contributes to
494 maintaining RbcS precursor accumulation, likely by promoting precursor stability and import

495 competence. Because MG132 treatment did not restore RbcS–GFP accumulation, the precise
496 degradation pathway remains unclear, suggesting that multiple quality-control mechanisms
497 may contribute to precursor turnover in the absence of ACTPK1. These findings support a
498 model in which ACTPK1-dependent phosphorylation contributes to maintaining precursor
499 accumulation and import competence, which in turn facilitates efficient Rubisco assembly and
500 photosynthetic function. In line with this interpretation, increased ACTPK1 activity in *mpk3*
501 knockout plants correlates with enhanced Rubisco accumulation and photosynthetic capacity,
502 whereas loss of ACTPK1 leads to reduced Rubisco levels and impaired photosynthetic
503 performance. However, the molecular mechanisms responsible for RbcS destabilization in the
504 absence of ACTPK1 remain to be elucidated, and future studies will be required to identify the
505 quality-control pathways that regulate precursor turnover. In addition, reduced RbcS transcript
506 levels in actpk1 mutants indicate that ACTPK1 may influence RbcS abundance through both
507 post-transcriptional and transcriptional mechanisms.

508 Genetic epistasis analysis establishes a linear signalling hierarchy in which ACTPK1 functions
509 downstream of MPK3. The *mpk3actpk1* double mutant phenocopies *actpk1* knockout plants in
510 terms of RbcS phosphorylation, Rubisco activity and photosynthetic capacity, demonstrating
511 that ACTPK1 is required for the photosynthetic effects of MPK3. Based on our findings under
512 non-stress growth conditions, we propose that the MPK3–ACTPK1 module may provide a
513 regulatory interface through which signalling pathways could modulate RbcS handling and
514 Rubisco biogenesis. Although the upstream signals that engage MPK3 in this context remain
515 unknown, it is plausible that modulation of MPK3 activity could influence ACTPK1-dependent
516 RbcS phosphorylation and thereby tune photosynthetic capacity.

517 Several mechanistic aspects of the MPK3–ACTPK1–RbcS pathway remain unresolved.
518 Although our data demonstrate that dynamic phosphorylation of the RbcS transit peptide is
519 required for efficient chloroplast targeting, the phosphatase responsible for RbcS
520 dephosphorylation has not yet been identified. In addition, while loss of ACTPK1 leads to rapid
521 loss of detectable RbcS and accelerated degradation in cell-free assays, the molecular
522 components of the cytosolic quality-control pathway responsible for RbcS turnover in the
523 absence of ACTPK1 remain unknown. Furthermore, although ACTPK1 directly
524 phosphorylates RbcS at Thr12 in vitro and genetic analyses support its role in vivo, the precise
525 molecular mechanism by which phosphorylation modulates precursor recognition, chaperone
526 engagement and TOC/TIC translocation remains to be defined. Finally, whether ACTPK1

527 regulates additional chloroplast-destined precursor proteins beyond RbcS is currently unknown
528 and will require systematic proteomic and genetic analyses.

529 In summary, our study reveals a signaling mechanism through which cytosolic MAPK activity
530 influences chloroplast protein import and photosynthetic performance. We identify ACTPK1
531 as a downstream target of MPK3 and show that this kinase regulates the stability and
532 chloroplast targeting competence of the Rubisco small subunit precursor through
533 phosphorylation of its transit peptide. Our results further indicate that efficient handling of the
534 RbcS precursor requires a dynamically regulated phosphorylation state rather than a
535 constitutive modification, highlighting transit peptide phosphorylation as a reversible
536 regulatory element in chloroplast protein trafficking. A simplified model of the findings has
537 been represented in Figure 8. Together, these findings uncover a signaling axis that links
538 cytosolic MAPK pathways with the control of Rubisco biogenesis and photosynthetic capacity,
539 providing a framework for understanding how cellular signaling networks coordinate
540 chloroplast function with broader physiological demands in plants.

541 **Materials and Methods**

542 **Transgene construct**

543 For generation of overexpression lines, full-length coding sequence (CDS) of *ACTPK1* was
544 amplified with 3xFLAG tag at 5' end and 4xMYC tag at 3' end was sandwiched between 35S
545 promoter and Nos terminator and cloned into binary vector pCAMBIA1300-CaMV 35S. The
546 pCAMBIA1300-35S-*ACTPK1* plasmid was introduced into rice *japonica* cultivar Taipea309
547 (Tp309) via *Agrobacterium*-mediated transformation using *Agrobacterium* strain EHA105.

548 *ACTPK1* knockout mutants were generated using CRISPR-Cas9 mediated gene editing in
549 japonica cultivar Tp309 background according to Rengasamy et al., 2024. A single guide RNA
550 (sgRNA) targeting the CDS region of *ACTPK1* gene (sgRNA:
551 GGGGACGGCGCGCGGACAAGAGC, PAM sequence: GGG) was designed and
552 synthesized as an oligonucleotide. The synthesized sgRNA was then cloned in pRGB32 vector
553 and introduced into 10-day-old rice Calli through *Agrobacterium*-mediated transformation.
554 The *MPK3-ACTPK1* double knockout was generated by mutating *ACTPK1* in *mpk3 ko*
555 background using CRISPR-Cas9 genome editing tool using the same sgRNA (sgRNA:
556 GGGGACGGCGCGCGGACAAGAGC).

557 **Plant growth conditions**

558 Rice seeds used for photosynthesis experiments were homozygous seeds of atleast T2
559 generation. Along with *ACTPK1 OE*, *actpk1 ko* and *mpk3-actpk1* double knockout,
560 dexamethasone (DEX) inducible MPK3 OE lines (*MPK3-23*, *MPK3-24*) and *mpk3 ko* (*mpk3*
561 *ko1*, *mpk3 ko2*) plants (both generated in *Oryza sativa* Tp309 cultivar) were used (Singh et al
562 2019, Banerjee et al., 2025). Seeds were germinated in petri plates having moist germination
563 paper for 7 days at 28 ºC, 16h light and 8h dark conditions. Seven days old seedlings were
564 transferred to one-fourth M.S. (Himedia) hydroponics media containing both micro and
565 macronutrients. The pH of the media solution was adjusted to 5.5, and media was renewed
566 every 3 days. Post 20 days, plants were transferred to pots and kept in a greenhouse at 28/22
567 ºC day and night air temperature, 70% relative humidity, a photoperiodic cycle of 16h light/8h
568 dark photoperiod, and ~500 µmol m^{-2} s^{-1} light intensity. The plants were maintained in pots in
569 greenhouse until maturity, and photosynthetic parameters were recorded from the middle
570 widest area of flag leaf at heading stage. For *MPK3 OE* lines, 1 um DEX and DMSO (mock)
571 were sprayed one day prior to taking photosynthetic readings (Singh et al., 2019).

572 **Photosynthesis rate and related physiological trait measurements**

573 Photosynthetic rate and its related physiological parameters were measured using Li-COR 6800
574 portable photosynthesis system on the flag leaf of rice plant at heading stage. The area of Li-
575 COR 6800 portable system leaf chamber was set at 2 cm^2 with a LED light source (LI-6400-
576 02B; LI-COR, Inc). To acquire the same leaf area, two young leaves were carefully placed in
577 leaf chamber without any overlap for plants having leaf width less than 2 cm^2 (Busch et al,
578 2018). For all the measurements, the conditions of leaf chamber were set as follows: 1500 µmol
579 m^{-2} s^{-1} light intensity (PAR), 400 µmol mol^{-1} CO_2 concentration, 300 µmol s^{-1} constant airflow,
580 70-80% relative humidity. Ten flag leaves from different plants were used to evaluate the net
581 photosynthesis rate (*A*), intercellular CO_2 concentration (*Ci*) and stomatal conductance to water
582 (*gs*).

583 For A/Ci curve, the leaves were first acclimatised to ambient CO_2 concentration of 400 µmol
584 mol^{-1} CO_2 and a constant PAR of 1500 µmol m^{-2} s^{-1} for 10 min and then the CO_2 concentration
585 was first gradually decreased from 400 to 50 (400, 300, 200, 150, 100, 50) µmol mol^{-1} CO_2 and
586 then leaf was stabilized at 400 µmol mol^{-1} CO_2 and again CO_2 concentration was increased
587 from 400 to 1400 (400, 600, 800, 1000, 1200 and 400) µmol mol^{-1} CO_2. The minimum and

588 maximum wait time between the subsequent readings was 60 and 120 sec respectively.
589 Readings were taken at constant PAR of 1500 µmol m^{-2} s^{-1}, flow rate of 500 µmol s^{-1}. The
590 maximum rate of Rubisco mediated carboxylation (*Vcmax*), electron transport rate (*J*) and
591 triose phosphate utilisation (*TPU*) were calculated by fitting A/Ci curve using Farquhar-von
592 Caemmerer-Berry (FvcB model) (Sharkey, 2015).

593 For light curve, the leaf was first acclimatised to constant saturating photosynthetic active
594 radiation (PAR) of 1500 µmol m^{-2} s^{-1} for about 10 min and then the PAR was decreased from
595 1500 to 100 (1500,1200,1000, 700, 500, 300 and 100) µmol m^{-2} s^{-1} at constant CO_2
596 concentration of 400 µmol mol^{-1} CO_2 and flow rate of 500 µmol s^{-1}. The minimum and
597 maximum wait time between the subsequent readings was 120 and 180 sec respectively.

598 All measurements were taken between 9.00 am to 11.00 am.

599 **Gene expression analysis**

600 Total RNA was isolated from leaf samples using RNeasy Plant mini kit (Qiagen) following
601 manufacturer's protocol. DNase treatment was given to 2 µg RNA using RNA free DNase I
602 (Qiagen) and subjected to first strand cDNA synthesis using RevertAid First Strand cDNA
603 synthesis kit (Thermo Scientific) per the manufacturer's protocol. Quantitative RT-PCR of
604 ACTPK1 and RbcS was carried out using Power SYBR Green PCR master mix (Applied
605 Biosystems). The conditions of thermocycler were set as follows: 94 °C for 10 min, 40 cycles
606 of 94 °C for 20 sec, 60 °C for 1 min. The housekeeping gene UBQ5 and Actin7 were used as
607 an internal control for normalization. Expression levels of examined genes were quantified
608 using relative quantitation method (ΔΔCT). The statistical significance was evaluated using t-
609 test. Data shown is the mean value of at least three biological repeats with SD. The primers
610 used for doing qRT-PCR are listed in supplemental Table 1.

611 **Site-directed mutagenesis**

612 Site-directed mutagenesis was performed using overlap extension PCR. Complementary
613 primers containing the desired mutation were designed. The target gene was amplified in two
614 fragments using gene-specific forward and mutation-specific reverse primers, and mutation-
615 specific forward and gene-specific reverse primers. Both amplicons were gel-purified and used
616 in overlap extension PCR with the following conditions: 98°C for 30 s, 55–58°C for 1 min,
617 72°C for 30 s/kb for 10 cycles. Gene-specific primers were then added for 35 additional cycles.

618 The final PCR product was gel-purified, verified by DNA sequencing, and cloned into the
619 target vector.

620 **Bacterial protein induction, purification and *in vitro* phosphorylation assay**

621 The full length CDS of *MPK3*, *MPK6*, *ACTPK1*, and *RbcS* were cloned in-frame with the
622 sequence of GST-tag in pGEX4-T-2 vector. Recombinant protein was induced in *Escherichia*
623 *coli BL21 Rosetta®* by adding 1mM IPTG at 22 °C. Induced recombinant proteins with GST-
624 tag were purified by affinity chromatography using GST-sepharose beads. Protein
625 concentration was determined using Bradford reagent (Sigma) and purity was analysed using
626 SDS-PAGE. *In vitro* phosphorylation assay was performed according to the method described
627 by Raghuram *et al*, 2015. Briefly, purified recombinant proteins of kinase and substrate (ratio
628 1:10) were incubated in kinase reaction buffer (25 mM Tris/Cl (pH 7.5), 10 mM $MgCl_2$, 5 mM
629 $MnCl_2$, 1 mM DTT, 1 mM β-glycerol phosphate, 1 mM Na_3VO_4, 25 mM ATP and 1 mCi [γ-
630 32P] ATP) for 30 min at 30 °C. The reaction was stopped by adding 6X SDS sample buffer
631 followed by heating at 95 °C for 5 min. The reaction samples were subjected to 12% SDS-
632 PAGE and exposed to phosphor screen followed by visualization using phosphor imager
633 (Typhoon, Phosphor Imaging System, GE Health Care, Life Sciences).

634 **Plant protein extraction and Immunoblot Analysis**

635 For SDS-PAGE, Proteins were extracted from rice seedlings using protein extraction buffer
636 (50 mM Tris HCl (pH 7.5), 5 mM EDTA, 5 mM EGTA, 150 mM NaCl, 1 mM DTT, 10 mM
637 Na_3VO_4, 10 mM NaF, 1mM PMSF, 2 mg/ml PVPP, 10% glycerol (v/v), 0.1% Nonidet P-40
638 (v/v) and 1× protease inhibitor cocktail (Sigma-Aldrich/Merck)). Extracted proteins were
639 quantified with Bradford reagent and ~40 µg was separated by 10/12% SDS-PAGE.
640 Specifically, 1 and 5 µg protein was resolved for RbcL and RbcS content quantification
641 respectively. Separated proteins were transferred to PVDF membrane for immunodetection.
642 The membranes were first blocked with 5% skimmed milk in TBST (10 mM Tris (pH 7.5), 500
643 mM NaCl, 0.05% Tween 20) for 2 h, then probed with anti RbcS (Agrisera, dilution 1:5000),
644 anti Actin (Sigma-Aldrich, dilution 1:5,000) antibody in TBST for 2 h at room temperature.
645 After two TBST washes (2 min each), membranes were incubated with anti-rabbit secondary
646 antibody (Thermofisher Scientific A11034) for 1.5 h. The membrane was again washed twice
647 with TBST (10 min each) and MQ water and visualized using Immobilon Western
648 chemiluminescent HRP substrate (BIORAD) as per manufacturer's instructions.

649 Chemiluminescence was detected with ChemiDoc system iBright 1500 (Amersham
650 Biosciences).
651 For quantification of Rubisco, Proteins were extracted using non-denaturing extraction buffer
652 (50 mM Tris HCl (pH 7.5), 50 mM NaCl, 1 mM DTT, 2 mg/ml PVPP, 10% glycerol (v/v),
653 0.1% Nonidet P-40 (v/v) and 1× protease inhibitor cocktail (Sigma-Aldrich/Merck). 1 µg
654 protein was resolved on 5-15% gradient BN-PAGE, transferred to PVDF membrane and
655 probed with anti-RbcL antibody.

656 ***In vivo* phosphorylation assay**

657 *In vivo* phosphorylation of RbcS was examined by mobility shift assay employing phos-tag
658 reagent. Proteins were extracted from WT, *mpk3 ko, ACTPK1 OE, actpk1 ko, mpk3actpk1 ko*
659 seedlings using protein extraction buffer (50 mM Tris HCl (pH 7.5), 150 mM NaCl, 1 mM
660 DTT, 10 mM NaF, 1mM PMSF, 10% glycerol (v/v) and 0.1% Nonidet P-40 (v/v)). Extracted
661 protein was separated by 12% (w/v) SDS-PAGE gel containing 100 µM phos-tag and 100 mM
662 $MnCl_2$. After electrophoresis, the gel was washed thrice, twice with transfer buffer containing
663 10 mM EDTA and once without EDTA for 10 min. Post washing, separated proteins were
664 transferred to nitrocellulose membrane using Trans-Blot SD cell (BIO-RAD) and membrane
665 was probed with α-RbcS (Agrisera) antibody. The membrane was again washed twice with
666 TBST (10 min each) and MQ water and visualized using Immobilon Western
667 chemiluminescent HRP substrate (BIORAD) as per manufacturer's instructions.
668 Chemiluminescence was detected with ChemiDoc system iBright 1500 (Amersham
669 Biosciences).

670 **Immuno-kinase (IP-kinase) assay**

671 Total protein was extracted from the 14 day old seedlings of WT, *mpk3 ko1* and *mpk3 ko2*
672 using the previously described protein extraction. Extracted proteins were quantified using
673 Bradford reagent, and 1 mg crude protein was incubated with 5 µg anti ACTPK1 antibody
674 (genescript) on a rocker at 4°C for 3 h. Subsequently, 50 µL Protein A Sepharose beads (50%
675 slurry, Pierce) were added and incubated on a rocker at 4°C for 1.5 h. Post incubation,
676 sepharose beads were washed with PBS-T (PBS with 0.05% Tween 20) thrice, resuspended in
677 kinase buffer containing 1 mCi [γ-^{32}P] ATP and 0.5 µg MBP, and incubated at 30°C for 30
678 min. Reactions were stopped with 3× SDS dye, boiled at 95°C for 5 min, and resolved by 12%

679 SDS-PAGE. Gels were exposed to a phosphor screen and visualized using a Typhoon phosphor
680 imager (GE Healthcare).

681 **Yeast two-hybrid assay**

682 The interaction between MPK3 and ACTPK1, and ACTPK1 and RbcS was examined using
683 the Matchmaker Gold Yeast Two-hybrid System (Takara Bio). Full-length CDS of MPK3,
684 MPK6, ACTPK1 and RbcS were cloned in pGBKT7 and pGADT7 vector (Clontech). Yeast
685 transformation with was performed using Fast Yeast Transformation kit (Gbiosciences; GZ-1)
686 (according to the manufacturer's protocol). The positive transformants were selected on double
687 dropout medium (Synthetic Defined (SD) /-Leu/-Trp)). The interaction assay was performed
688 by plating the selected transformants on quadruple dropout medium ((SD)/-Ade/-His/-Leu/-
689 Trp) followed by incubation at 30 °C for 36–48h. The fully grown colonies after the incubation
690 were marked as positive interactions.

691 **Subcellular localisation and Bimolecular Fluorescence Complementation assay (BiFC)**

692 For subcellular localisation, full-length CDS of MPK3 and RbcS was cloned in pGWB5 vector.
693 The resulting construct (MPK3-pGWB5) was transformed into *Agrobacterium* strain EHA105
694 and infiltrated in young and healthy leaves of *Nicotiana benthamiana*. The plasmid of RbcS-
695 pGWB5, $RbcS^{T12D}$-pGWB5 and $RbcS^{T12A}$-pGWB5 was introduced in rice protoplast using
696 PEG-mediated transformation (citation). Localisation was analysed post 48h for *Nicotiana*
697 *benthamiana* and post 16h for rice protoplast using a Leica TCS SP8 AOBS Laser Scanning
698 Microscope (Leica Microsystems) using GFP filters with fluorescence excitation at 514 nm
699 and emission at 527 nm.

700 For BiFC, full length CDS of MPK3, ACTPK1 and RbcS was cloned into pSITE-nEYFP-C1
701 (Cd3-1648) and pSITE-cEYFP-N1 (Cd3-1651) vectors. The resulting constructs were
702 transformed into *Agrobacterium* strain EHA105 and infiltrated in young and healthy leaves of
703 *Nicotiana benthamiana*. Interaction was analysed post 48h using a Leica TCS SP8 AOBS Laser
704 Scanning Microscope (Leica Microsystems) using YFP filters with fluorescence excitation at
705 514 nm and emission at 527 nm.

706 **Co-immunoprecipitation (Co-IP) assay**

707 Flag-tagged ACTPK1 (pCAMBIA1300-35S-Flag-*ACTPK1*) and GFP-tagged MPK3 (MPK3-
708 pGWB5) were co-expressed in *Nicotiana benthamiana* leaves via *Agrobacterium*-mediated
709 infiltration. Proteins were extracted 48 h post-infiltration using protein extraction buffer.
710 Proteins (1 mg) were incubated with 5 µg anti-Flag antibody (Sigma-Aldrich) at 4°C for 3 h
711 with rocking, followed by 50 µL Protein A Sepharose beads (50% slurry, Pierce) for 1.5 h.
712 Beads were washed thrice with PBS-T (PBS, 0.05% Tween 20), eluted with 2× SDS sample
713 buffer, boiled at 95°C for 5 min, and resolved on 10% SDS-PAGE. Proteins were transferred
714 to PVDF, blocked with 5% skimmed milk in TBST (10 mM Tris, pH 7.5; 500 mM NaCl; 0.05%
715 Tween 20) for 2 h, and probed with anti-GFP antibody (Abcam) for 2 h at room temperature.
716 After two 10-min TBST washes, membranes were incubated with HRP-conjugated secondary
717 antibody for 1.5 h, washed twice with TBST and MQ water, and visualized using Immobilon
718 Western chemiluminescent HRP substrate (BIORAD) as per manufacturer's instructions.
719 Chemiluminescence was detected with ChemiDoc system iBright 1500 (Amersham
720 Biosciences).

721 **Cell-free degradation assay**

722 Total protein was extracted from 14-day-old rice seedlings (WT, *mpk3 ko*, *actpk1 ko*) by
723 grinding 1 g tissue in liquid nitrogen and homogenizing in 1 mL ice-cold protein extraction
724 buffer. Extracted proteins were quantified using Bradford reagent. Crude extract (100 µg) was
725 incubated with 1 µg recombinant GST-tagged RbcS in 100 µL reaction buffer (50 mM Tris-
726 HCl, (pH 7.5), 5 mM $MgCl_2$, 5 mM ATP, and 1 mM DTT) at room temperature. Aliquots (20
727 µL) were collected at 0, 5, 10, 30, 60, and 120 min, stopped with 2× SDS sample buffer, boiled
728 at 95°C for 5 min, and resolved on 12% SDS-PAGE. Proteins were transferred to nitrocellulose
729 membrane and probed with anti-GST antibody (Thermofischer), and visualized using
730 Immobilon Western chemiluminescent HRP substrate (BIORAD) as per manufacturer's
731 instructions. Chemiluminescence was detected with ChemiDoc system iBright 1500
732 (Amersham Biosciences). Band intensity was quantified with ImageJ.

733 **Rubisco activity measurements**

734 Rubisco activity assay was performed according to Sharwood et al., (2016). Briefly, Leaf
735 tissues were excised (2 cm^2) from the middle widest part of the same leaf from which
736 photosynthesis parameters were recorded, pulverized and homogenized in 1 mL ice-cold
737 extraction buffer (5 mM DTT, 10 mg ml^{-1} PVPP, 2 mg ml^{-1} BSA, 2 mg ml^{-1} PEG, 2% (v/v)

738 Tween-80, 12 mM 6-aminocaproic acid, 2.4 mM benzamidine in HEPES stock) at 4 °C. The
739 homogenate was centrifuged at 15,000 × g at 4°C for 1 min, and supernatant was incubated
740 with freshly prepared BMEC buffer (100 mM Bicine–NaOH, pH 8.2, 20 mM $MgCl_2$, 1 mM
741 Na_2-EDTA, and 10 mM $NaHCO_3$) in a 9:1 ratio (e.g. 900 µl leaf extract to 100 µl BMEC) at
742 25 °C for 25 min, to activate the Rubisco enzyme. To assess the activity, 50 µl of leaf extract
743 was incubated with 1550 µl of EME buffer (100 mM EPPS–NaOH (pH 8.2), 20 mM $MgCl_2$, 1
744 mM Na_2-EDTA), 40 µl of 10 mM NADH (final concentration 200 µM), 80 µl of 250 mM
745 $NaH_{12}CO_3$ (final concentration 10 mM), 200 µl of ATP/phosphocreatine (final concentrations
746 1 mM and 5 mM, respectively), 40 µl of coupling enzymes (carbonic anhydrase 500 U,
747 glyceraldehyde-3-phosphate dehydrogenase 50 U, 3-phosphoglycerate kinase 50 U, triose-
748 phosphate isomerase/glycerol-3-phosphate dehydrogenase 400/40 U), and 40 µl of 25 mM
749 RuBP (final concentration 500 µM), and the decrease of absorbance was monitored at 340 nm
750 for 180 s using a UV–Vis spectrophotometer. The Rubisco carboxylation rate was calculated
751 using the equation:
752 RuBP− use (µmol s^{-1}) = (ΔOD340 ∗ Vol)/6.18 X 4
753 assuming an extinction coefficient of 6.18 µmol ml^{-1} cm^{-1} for NADH oxidation at 340 nm.
754 ΔOD340 is the rate of change of absorbance at 340 nm per second, and Vol is assay volume (1
755 ml). The equation accounts for the four NADH molecules oxidized per RuBP carboxylated by
756 Rubisco. The activity of Rubisco (*Vcmax*) is calculated as:
757 *Vcmax* (µmol m^{-2} s^{-1}) = ((RuBP−use; µmol s^{-1}) (EV; µl) (10000 cm^2/m^2))/(LA; cm^2) (Sample
758 volume; µl)
759 where EV is extraction volume and LA is leaf area.

760 **Rice protoplast isolation and PEG mediated transformation**

761 Protoplast from rice seedlings were isolated according to Zhang et al., 2011. Seeds of WT,
762 *mpk3 ko* and *actpk1 ko* were surface sterilized and germinated on half-strength MS solid
763 medium. Seven- to ten-day-old seedlings were chopped into 0.5 mm strips in 0.5 M mannitol,
764 incubated for 10 min, and transferred to enzyme solution (0.4 M mannitol, 1.5% Cellulase RS
765 (Yakult), 0.75% Macerozyme (Yakult), 20 mM MES (pH 5.7), 10 mM $CaCl_2$, 20 mM KCl,
766 0.1% BSA) for 3-4 h at 80 rpm at room temperature. The reaction was stopped with equal
767 volume of W5 buffer (154 mM NaCl, 125 mM $CaCl_2$, 5 mM KCl, 2 mM MES (pH 5.7)),
768 shaken for 10 s to release protoplasts, and filtered through a 100 µm nylon mesh. Additional 5
769 ml W5 buffer was added to the strips, strained again and centrifuged at 1500 rpm for 3 min at

770 room temperature. The pellet was washed with 5 mL W5 buffer, resuspended in MMG buffer
771 (4 mM MES (pH 5.7), 0.4 M Mannitol, 15 mM $MgCl_2$), and protoplast quality was assessed
772 under a light microscope.

773 PEG-mediated transient transformation of protoplasts was performed according to Shen et al.,
774 (2014). Approximately 100 µL of protoplasts were mixed with 5–10 µg plasmid of RbcS-
775 pGWB5, $RbcS^{T12D}$-pGWB5 and $RbcS^{T12A}$-pGWB5 in a microcentrifuge tube by gentle
776 tapping. Subsequently, 110 µL of PEG solution (40% PEG_{4000} (Fluka), 0.2 M Mannitol, 100
777 mM $CaCl_2$) was added, mixed by tapping, and incubated in the dark at room temperature for
778 20 min. The solution was diluted with 440 µL W5 buffer, centrifuged at 1500 rpm for 3 min,
779 and the pellet was resuspended in 1 mL WI solution (4 mM MES, 0.5 M mannitol, 20 mM
780 KCl). After 16 h incubation in the dark, transformed protoplasts were analysed using a Leica
781 TCS SP8 AOBS Laser Scanning Microscope (Leica Microsystems) using GFP and chloroplast
782 autofluorescence filters.

783 For phosphatase inhibitor treatment, protoplasts were exposed to 50nm okadaic acid after 16 h
784 of transfection for 30 mins. Afterwards protoplast were analysed using a Leica TCS SP8 AOBS
785 Laser Scanning Microscope (Leica Microsystems) using GFP and chloroplast autofluorescence
786 filters.

787 **Pigment content measurement**

788 Pigment content were measured according to procedure described by Porra et al., (1989). Leaf
789 samples (1 g) were harvested post photosynthetic parameters measurements, and chlorophyll
790 and total carotenoid was extracted in 80% ice-cold acetone (aqueous). Chlorophyll and
791 carotenoid contents were measured spectrophotometrically and calculated according to Arnon,
792 1949.

793 **Statistical analysis**

794 Student t-test and one-way analysis of variance (ANOVA) were performed to determine
795 significant differences indicated as *P<0.05, **P< 0.005, and ***P< 0.0005. Details of
796 statistical analysis and sample sizes in each experiment are mentioned in the figure legends.
797 ImageJ was used to quantify the intensities of bands in the immunoblots.

798 **Locus Ids of gene**

MPK3 (LOC_Os03g17700); MPK6 (LOC_Os06g06090); ACTPK1 (LOC_Os02g02780); RbcS3 (LOC_Os12g17600)

Supplemental figure and table legends:

Fig S1. Photosynthetic pigments and parameters in WT, *MPK3 OE* (*MPK3-23*, *MPK3-24*) and *mpk3 ko* (*mpk3 ko1*, *mpk3 ko2*) lines.

Fig. S2 Localisation of MPK3 and interaction and phosphorylation of RbcS with MPK3 and MPK6.

Fig. S3 ACTPK1 is a Raf-like MAPKKK exhibiting homology and sequence similarity with *At*STY8, *At*STY17 and *At*STY46, and contains multiple MAPK phosphorylation motifs.

Fig. S4 Lysine at 332 and 428 are crucial for trans- and auto-phosphorylation activity of ACTPK1 and ACTPK1 do not phosphorylate MPK3.

Fig. S5 ACTPK1 phosphorylates RbcS at Thr12.

Fig. S6 Localization of RbcS-GFP in *mpk3 ko* and *actpk1 ko* protoplasts.

Fig. S7 Development of *ACTPK1 OE* and *actpk1 ko* lines.

Fig. S8 Intercellular CO_2 concentration in flag leaf of WT, *ACTPK1 OE* and *actpk1 ko* plants.

Fig. S9ACTPK1 regulates vegetative growth, flag leaf angle, flowering time and seed architecture.

Supplemental Table1: Table containing the list of primers used in this study.

Acknowledgments

SJ and RB are thankful to the Department of Biotechnology (DBT) for the fellowship. GB, MB and PS are thankful to the Council of Scientific and Industrial Research (CSIR) for the fellowship. AKS thanks Sir JC Bose Fellowship from the Anusandhan National Research Foundation, Department of Science and Technology, Government of India (File no.: JCB/2020/000041). The work is supported by the grant from the Anusandhan National Research Foundation, Department of Science and Technology, Government of India (File No.: CRG/2023/001751). The authors also acknowledge the Gene Functional Analysis Platform for Crops, Confocal Facility, DNA sequencing facility, Radioisotope facility and the Central Instrumentation Facility of NIPGR, New Delhi, India. The authors declare no conflict of interest.

Authors' contribution

SJ and AKS planned the study and designed the experiments. SJ and RB generated and screened transgenic plants and recorded the photosynthetic parameters. SJ and GB carried out the molecular biology experiments. SJ, MB and MM recorded and analysed the phenotypic traits of transgenic plants. PS screened the *mpk3actpk1* double knockout plants. SJ and AKS analysed data and wrote the manuscript. SJ wrote the initial draft and AKS finalise the draft. All authors read and approved the final manuscript.

Declaration of competing interest

The authors declare no competing interests.

References

Allen, D. J., & Ort, D. R. (2001). Impacts of chilling temperatures on photosynthesis in warm-climate plants. *Trends in plant science*, *6*(1), 36-42.

Andersson, I., & Backlund, A. (2008). Structure and function of Rubisco. *Plant Physiology and Biochemistry*, *46*(3), 275-291.

Arnon, D. I. (1949). Copper enzymes in isolated chloroplasts. Polyphenoloxidase in Beta vulgaris. *Plant physiology*, *24*(1), 1.

Banerjee, G., Jonwal, S., Rengasamy, B., Pal, U., Singh, D., Mohit, M., & Sinha, A. K. (2025). KRP3 Stability Controls Rice Plant Architecture and Productivity via MPK3-Mediated Phosphorylation. *Plant Biotechnology Journal*.

Beier, M. P., Obara, M., Taniai, A., Sawa, Y., Ishizawa, J., Yoshida, H., ... & Hayakawa, T. (2018). Lack of ACTPK 1, an STY kinase, enhances ammonium uptake and use, and promotes growth of rice seedlings under sufficient external ammonium. *The Plant Journal*, *93*(6), 992-1006.

Bellafiore, S., Barneche, F., Peltier, G., & Rochaix, J. D. (2005). State transitions and light adaptation require chloroplast thylakoid protein kinase STN7. *Nature*, *433*(7028), 892-895.

Borba, A. R., Reyna-Llorens, I., Dickinson, P. J., Steed, G., Gouveia, P., Górska, A. M., ... & Hibberd, J. M. (2023). Compartmentation of photosynthesis gene expression in C4 maize depends on time of day. *Plant Physiology*, *193*(4), 2306-2320.

Bruce, B. D. (2000). Chloroplast transit peptides: structure, function and evolution. *Trends in cell biology*, *10*(10), 440-447.

Busch, F. A., Sage, R. F., & Farquhar, G. D. (2018). Plants increase CO2 uptake by assimilating nitrogen via the photorespiratory pathway. *Nature plants*, *4*(1), 46-54.

Covshoff, S., & Hibberd, J. M. (2012). Integrating C4 photosynthesis into C3 crops to increase yield potential. *Current opinion in biotechnology*, *23*(2), 209-214.

Eichberg, J., & Iyer, S. (1996). Phosphorylation of myelin proteins: recent advances. *Neurochemical research*, *21*(4), 527-535.

Evans, J. R. (2013). Improving photosynthesis. *Plant physiology*, *162*(4), 1780-1793.

Evans, J. R. (2021). Mesophyll conductance: walls, membranes and spatial complexity. *New Phytologist*, *229*(4), 1864-1876.

Feiz, L., Williams-Carrier, R., Wostrikoff, K., Belcher, S., Barkan, A., & Stern, D. B. (2012). Ribulose-1, 5-bis-phosphate carboxylase/oxygenase accumulation factor1 is required for holoenzyme assembly in maize. *The Plant Cell*, *24*(8), 3435-3446.

Gao, J., Li, S., Lei, Y., Wang, Q., Ning, Z., Lu, Z., ... & Yang, W. (2024). Delayed photosynthesis response causes carbon assimilation reduction in soybean under fluctuating light. *Journal of Integrative Agriculture*.

Gao, X., Xin, D., Zhao, Y., Li, J., Cao, Y., Zhang, S., & Guo, J. (2024). Potential molecular mechanism of photosynthesis regulation by PeMPK7 in poplar under para-hydroxybenzoic acid stress. *Ecotoxicology and Environmental Safety*, *276*, 116329.

Gawroński, P., Witoń, D., Vashutina, K., Bederska, M., Betliński, B., Rusaczonek, A., & Karpiński, S. (2014). Mitogen-activated protein kinase 4 is a salicylic acid-independent regulator of growth but not of photosynthesis in Arabidopsis. *Molecular Plant*, *7*(7), 1151-1166.

Grabsztunowicz, M., Koskela, M. M., & Mulo, P. (2017). Post-translational modifications in regulation of chloroplast function: recent advances. *Frontiers in plant science*, *8*, 240.

Hamel, L. P., Nicole, M. C., Sritubtim, S., Morency, M. J., Ellis, M., Ehlting, J., ... & Ellis, B. E. (2006). Ancient signals: comparative genomics of plant MAPK and MAPKK gene families. *Trends in plant science*, *11*(4), 192-198.

Hashimoto-Sugimoto, M., Negi, J., Monda, K., Higaki, T., Isogai, Y., Nakano, T., ... & Iba, K. (2016). Dominant and recessive mutations in the Raf-like kinase HT1 gene completely disrupt stomatal responses to CO2 in Arabidopsis. *Journal of Experimental Botany*, *67*(11), 3251-3261.

Hauser, T., Popilka, L., Hartl, F. U., & Hayer-Hartl, M. (2015). Role of auxiliary proteins in Rubisco biogenesis and function. *Nature Plants*, *1*(6), 1-11.

Hettenhausen, C., Baldwin, I. T., & Wu, J. (2012). Silencing MPK4 in Nicotiana attenuata enhances photosynthesis and seed production but compromises abscisic acid-induced stomatal closure and guard cell-mediated resistance to Pseudomonas syringae pv tomato DC3000. *Plant Physiology*, *158*(2), 759-776.

Hiyama, A., Takemiya, A., Munemasa, S., Okuma, E., Sugiyama, N., Tada, Y., ... & Shimazaki, K. I. (2017). Blue light and CO2 signals converge to regulate light-induced stomatal opening. *Nature communications*, *8*(1), 1284.

Houtz, R. L., Stults, J. T., Mulligan, R. M., & Tolbert, N. E. (1989). Post-translational modifications in the large subunit of ribulose bisphosphate carboxylase/oxygenase. *Proceedings of the National Academy of Sciences*, *86*(6), 1855-1859.

Jarvis, P., & López-Juez, E. (2013). Biogenesis and homeostasis of chloroplasts and other plastids. *Nature Reviews Molecular Cell Biology*, *14*(12), 787-802.

Jarvis, P., & Robinson, C. (2004). Mechanisms of protein import and routing in chloroplasts. *Current Biology*, *14*(24), R1064-R1077.

Jonwal, S., Verma, N., & Sinha, A. K. (2022). Regulation of photosynthetic light reaction proteins via reversible phosphorylation. *Plant Science*, *321*, 111312.

Jonwal, S., Rengasamy, B., & Sinha, A. K. (2023). Regulation of photosynthesis by mitogen-activated protein kinase in rice: antagonistic adjustment by OsMPK3 and OsMPK6. *Physiology and Molecular Biology of Plants*, *29*(9), 1247-1259.

Tõldsepp, K., Zhang, J., Takahashi, Y., Sindarovska, Y., Hõrak, H., Ceciliato, P. H., ... & Schroeder, J. I. (2018). Mitogen-activated protein kinases MPK 4 and MPK 12 are key components mediating CO 2-induced stomatal movements. *The Plant Journal*, *96*(5), 1018-1035.

Kalaji, H. M., Jajoo, A., Oukarroum, A., Brestic, M., Zivcak, M., Samborska, I. A., ... & Ladle, R. J. (2016). Chlorophyll a fluorescence as a tool to monitor physiological status of plants under abiotic stress conditions. *Acta physiologiae plantarum*, *38*(4), 102.

Lamberti, G., Gügel, I. L., Meurer, J., Soll, J., & Schwenkert, S. (2011). The cytosolic kinases STY8, STY17, and STY46 are involved in chloroplast differentiation in Arabidopsis. *Plant physiology*, *157*(1), 70-85.

Lee, D. W., Jung, C., & Hwang, I. (2013). Cytosolic events involved in chloroplast protein targeting. *Biochimica et Biophysica Acta (BBA)-Molecular Cell Research*, *1833*(2), 245-252.

Lee, D. W., Lee, S., Oh, Y. J., & Hwang, I. (2009). Multiple sequence motifs in the rubisco small subunit transit peptide independently contribute to Toc159-dependent import of proteins into chloroplasts. *Plant Physiology*, *151*(1), 129-141.

Lee, S., Lee, D. W., Lee, Y., Mayer, U., Stierhof, Y. D., Lee, S., ... & Hwang, I. (2009). Heat shock protein cognate 70-4 and an E3 ubiquitin ligase, CHIP, mediate plastid-destined precursor degradation through the ubiquitin-26S proteasome system in Arabidopsis. *The Plant Cell*, *21*(12), 3984-4001.

Li, Y., Gao, Y., Xu, X., Shen, Q., & Guo, S. (2009). Light-saturated photosynthetic rate in high-nitrogen rice (Oryza sativa L.) leaves is related to chloroplastic CO2 concentration. *Journal of Experimental Botany*, *60*(8), 2351-2360.

Long, S. P., ZHU, X. G., Naidu, S. L., & Ort, D. R. (2006). Can improvement in photosynthesis increase crop yields?. *Plant, cell & environment*, *29*(3), 315-330.

Hashimoto, M., Negi, J., Young, J., Israelsson, M., Schroeder, J. I., & Iba, K. (2006). Arabidopsis HT1 kinase controls stomatal movements in response to CO2. *Nature cell biology*, *8*(4), 391-397.

Manna, M., Rengasamy, B., & Sinha, A. K. (2023). Revisiting the role of MAPK signalling pathway in plants and its manipulation for crop improvement. *Plant, Cell & Environment*, *46*(8), 2277-2295.

Mathan, J., Bhattacharya, J., & Ranjan, A. (2016). Enhancing crop yield by optimizing plant developmental features. *Development*, *143*(18), 3283-3294.

May, T., & Soll, J. (2000). 14-3-3 proteins form a guidance complex with chloroplast precursor proteins in plants. *The Plant Cell*, *12*(1), 53-63.

Murchie, E. H., & Lawson, T. (2013). Chlorophyll fluorescence analysis: a guide to good practice and understanding some new applications. *Journal of experimental botany*, *64*(13), 3983-3998.

Murchie, E. H., & Niyogi, K. K. (2011). Manipulation of photoprotection to improve plant photosynthesis. *Plant physiology*, *155*(1), 86-92.

Nakagami, H., Kiegerl, S., & Hirt, H. (2004). OMTK1, a novel MAPKKK, channels oxidative stress signaling through direct MAPK interaction. *Journal of Biological Chemistry*, *279*(26), 26959-26966.

Ort, D. R., Merchant, S. S., Alric, J., Barkan, A., Blankenship, R. E., Bock, R., ... & Zhu, X. G. (2015). Redesigning photosynthesis to sustainably meet global food and bioenergy demand. *Proceedings of the national academy of sciences*, *112*(28), 8529-8536.

Parry, M. A. J., Madgwick, P. J., Carvalho, J. F. C., & Andralojc, P. J. (2007). Prospects for increasing photosynthesis by overcoming the limitations of Rubisco. *The Journal of Agricultural Science*, *145*(1), 31.

Porra, R. J., Thompson, W. A., & Kriedemann, P. E. (1989). Determination of accurate extinction coefficients and simultaneous equations for assaying chlorophylls a and b extracted with four different solvents: verification of the concentration of chlorophyll standards by atomic absorption spectroscopy. *Biochimica et Biophysica Acta (BBA)-Bioenergetics*, *975*(3), 384-394.

Puthiyaveetil, S., & Allen, J. F. (2009). Chloroplast two-component systems: evolution of the link between photosynthesis and gene expression. *Proceedings of the Royal Society B: Biological Sciences*, *276*(1665), 2133-2145.

Puthiyaveetil, S., Ibrahim, I. M., Jeličić, B., Tomašić, A., Fulgosi, H., & Allen, J. F. (2010). Transcriptional control of photosynthesis genes: the evolutionarily conserved regulatory mechanism in plastid genome function. *Genome biology and evolution*, *2*, 888-896.

Raghuram, B., Sheikh, A. H., Rustagi, Y., & Sinha, A. K. (2015). Micro RNA biogenesis factor DRB 1 is a phosphorylation target of mitogen activated protein kinase MPK 3 in both rice and Arabidopsis. *The FEBS journal*, *282*(3), 521-536.

Rao, K. P., Richa, T. A. M. B. I., Kumar, K. U. N. D. A. N., Raghuram, B. A. D. M. I., & Sinha, A. K. (2010). In silico analysis reveals 75 members of mitogen-activated protein kinase kinase kinase gene family in rice. *DNA research*, *17*(3), 139-153.

Reiland, S., Finazzi, G., Endler, A., Willig, A., Baerenfaller, K., Grossmann, J., ... & Baginsky, S. (2011). Comparative phosphoproteome profiling reveals a function of the STN8 kinase in fine-tuning of cyclic electron flow (CEF). *Proceedings of the National Academy of Sciences*, *108*(31), 12955-12960.

Reiland, S., Messerli, G., Baerenfaller, K., Gerrits, B., Endler, A., Grossmann, J., ... & Baginsky, S. (2009). Large-scale Arabidopsis phosphoproteome profiling reveals novel chloroplast kinase substrates and phosphorylation networks. *Plant physiology*, *150*(2), 889-903.

Rengasamy, B., Manna, M., Jonwal, S., Sathiyabama, M., Thajuddin, N. B., & Sinha, A. K. (2024). A simplified and improved protocol of rice transformation to cater wide range of rice cultivars. *Protoplasma*, *261*(4), 641-654.

Rochaix, J. D. (2014). Regulation and dynamics of the light-harvesting system. *Annual review of plant biology*, *65*, 287-309.

Rodriguez, M. C., Petersen, M., & Mundy, J. (2010). Mitogen-activated protein kinase signaling in plants. *Annual Review of Plant Biology, 61*, 621-649.

Rudrabhatla, P., Reddy, M. M., & Rajasekharan, R. (2006). Genome-wide analysis and experimentation of plant serine/threonine/tyrosine-specific protein kinases. *Plant Molecular Biology*, *60*(2), 293-319.

Schönberg, A., & Baginsky, S. (2012). Signal integration by chloroplast phosphorylation networks: an update. *Frontiers in plant science*, *3*, 256.

Schönberg, A., Rödiger, A., Mehwald, W., Galonska, J., Christ, G., Helm, S., ... & Baginsky, S. (2017). Identification of STN7/STN8 kinase targets reveals connections between electron transport, metabolism and gene expression. *The Plant Journal*, *90*(6), 1176-1186.

Sharkey, T. D. (2015). What gas exchange data can tell us about photosynthesis. *Plant, cell & environment*, *39*(6), 1161-1163.

Sharkey, T. D., Bernacchi, C. J., Farquhar, G. D., & Singsaas, E. L. (2007). Fitting photosynthetic carbon dioxide response curves for C3 leaves. *Plant, cell & environment*, *30*(9), 1035-1040.

Sharma, A., Kumar, V., Shahzad, B., Ramakrishnan, M., Singh Sidhu, G. P., Bali, A. S., ... & Zheng, B. (2020). Photosynthetic response of plants under different abiotic stresses: a review. *Journal of Plant Growth Regulation*, *39*(2), 509-531.

Shen, J., Fu, J., Ma, J., Wang, X., Gao, C., Zhuang, C., ... & Jiang, L. (2014). Isolation, culture, and transient transformation of plant protoplasts. *Current protocols in cell biology*, *63*(1), 2-8.

Shilpha, J., Song, J., & Jeong, B. R. (2023). Ammonium phytotoxicity and tolerance: An insight into ammonium nutrition to improve crop productivity. *Agronomy*, *13*(6), 1487.

Simkin, A. J., López-Calcagno, P. E., & Raines, C. A. (2019). Feeding the world: improving photosynthetic efficiency for sustainable crop production. *Journal of Experimental Botany*, *70*(4), 1119-1140.

Singh, P., Ara, H., Tayyeba, S., Pandey, C., & Sinha, A. K. (2019). Development of efficient protocol for rice transformation overexpressing MAP kinase and their effect on root phenotypic traits. *Protoplasma*, *256*(4), 997-1011.

Sinha, A. K., Jaggi, M., Raghuram, B., & Tuteja, N. (2011). Mitogen-activated protein kinase signaling in plants under abiotic stress. *Plant signaling & behavior*, *6*(2), 196-203.

Spreitzer, R. J. (2003). Role of the small subunit in ribulose-1, 5-bisphosphate carboxylase/oxygenase. *Archives of biochemistry and biophysics*, *414*(2), 141-149.

Su J, Yang L, Zhu Q, Wu H, He Y, Liu Y et al (2018). Active photosynthetic inhibition mediated by MPK3/MPK6 is critical to effector-triggered immunity. *PLoS biology*, *16*(5), e2004122.

Suzuki, Y., Ohkubo, M., Hatakeyama, H., Ohashi, K., Yoshizawa, R., Kojima, S., ... & Makino, A. (2007). Increased Rubisco content in transgenic rice transformed with the 'sense'rbcS gene.

Takahashi, Y., Bosmans, K.C., Hsu, P.K., Paul, K., Seitz, C., Yeh, C.Y., Wang, Y.S., Yarmolinsky, D., Sierla, M., Vahisalu, T. and Waszczak, C., (2022). Stomatal CO2/bicarbonate sensor consists of two interacting protein kinases, Raf-like HT1 and non-kinase-activity requiring MPK12/MPK4. *Science Advances*, *8*(49), p.eabq6161.

Terashima, I., Hanba, Y. T., Tholen, D., & Niinemets, Ü. (2011). Leaf functional anatomy in relation to photosynthesis. *Plant physiology*, *155*(1), 108-116.

Tikkanen, M., & Aro, E. M. (2012). Thylakoid protein phosphorylation in dynamic regulation of photosystem II in higher plants. *Biochimica et Biophysica Acta (BBA)-Bioenergetics*, *1817*(1), 232-238.

Von Caemmerer, S. (2000). *Biochemical models of leaf photosynthesis*. Csiro publishing.

Waegemann, K., & Soll, J. (1996). Phosphorylation of the transit sequence of chloroplast precursor proteins. *Journal of Biological Chemistry*, *271*(11), 6545-6554.

Witoń, D., Gawroński, P., Czarnocka, W., Ślesak, I., Rusaczonek, A., Sujkowska-Rybkowska, M., ... & Karpiński, S. (2016). Mitogen activated protein kinase 4 (MPK4) influences growth in Populus tremula L.× tremuloides. *Environmental and Experimental Botany*, *130*, 189-205.

Witoń, D., Sujkowska-Rybkowska, M., Dąbrowska-Bronk, J., Czarnocka, W., Bernacki, M., Szechyńska-Hebda, M., & Karpiński, S. (2021). MITOGEN-ACTIVATED PROTEIN KINASE 4 impacts leaf development, temperature, and stomatal movement in hybrid aspen. *Plant Physiology*, *186*(4), 2190-2204.

1050 Xiong, D. (2024). Perspectives of improving rice photosynthesis for higher grain
1051 yield. *Crop and Environment*, *3*(3), 123-137.

1052 Zhang, Y., Su, J., Duan, S., Ao, Y., Dai, J., Liu, J., ... & Wang, H. (2011). A highly efficient
1053 rice green tissue protoplast system for transient gene expression and studying
1054 light/chloroplast-related processes. *Plant methods*, *7*(1), 30.

1055 Zhu, X. G., Long, S. P., & Ort, D. R. (2010). Improving photosynthetic efficiency for
1056 greater yield. *Annual review of plant biology*, *61*(1), 235-261.

1057 Zhu, X., Zhang, N., Liu, X., Li, S., Yang, J., Hong, X., ... & Si, H. (2021). Mitogen-
1058 activated protein kinase 11 (MAPK11) maintains growth and photosynthesis of potato plant
1059 under drought condition. *Plant Cell Reports*, *40*, 491-506.

1060 Zhu, X., Zhang, N., Liu, X., Wang, S., Li, S., Yang, J., ... & Si, H. (2020). StMAPK3
1061 controls oxidase activity, photosynthesis and stomatal aperture under salinity and osmosis
1062 stress in potato. *Plant Physiology and Biochemistry*, *156*, 167-177.

1063

1064 **Main file Table and their legends:**

1065 **Table 1: CO_2-saturated maximum photosynthesis (A_{max}), maximum *in vivo* Rubisco activity**
1066 **(V_{cmax}), maximum electron transport rate (J), and maximum rate of triose phosphate**
1067 **utilization (*TPU*) of WT, *MPK3 OE* and *mpk3 ko* lines through A/C_i curve analysis.**

	Amean	*Amax*	*Vcmax*	*J*	*TPU*
WT	25.17 ± 2.34	36.18 ± 1.37	110.2 ± 5.58	142.4 ± 8.23	9.28 ± 0.38
MPK3-23 MOCK	25.48 ± 1.8	35.16 ± 1.6	88.29 ± 6.348	133.16 ± 5.75	8.73 ± 0.45
MPK3-23 DEX	17.75 ± 2.34	26.53 ± 3.2	61.77 ± 9.32	101.89 ± 11.5	6.94 ± 0.688
MPK3-24 MOCK	24.02 ± 3.10	34.22 ± 0.87	88.368 ± 9.23	132.72 ± 7.9	8.73 ± .078
MPK3-24 DEX	17.67 ± 1.43	28.57 ± 0.51	68.79 ± 10.83	116.92 ± 4.18	7.6 ± 0.17
mpk3 ko1	29.78 ± 1.75	40.83 ± 1.41	126.3 ± 3.2	165.12 ± 6.58	10.66 ± 0.4
mpk3 ko2	30.48 ± 1.28	41.8 ± 0.4	126.56 ± 2.54	163.65 ± 1.9	10.66 ± 0.02

1068 **Table 2: CO_2-saturated maximum photosynthesis (A_{max}), maximum *in vivo* Rubisco activity**
1069 **(V_{cmax}), maximum electron transport rate (J), and maximum rate of triose phosphate**
1070 **utilization (*TPU*) of WT, *ACTPK1 OE* and *actpk1 ko* lines through A/C_i curve analysis.**

	Amean	*Amax*	*Vcmax*	*J*	*TPU*
WT	22.27 ± 1.12	38.8 ± 1.08	88.18 ± 3.14	130.36 ± 7.36	9.5 ± 0.31
ACTPK1 OE19	21.89 ± 0.55	41.34 ± 0.37	88.25 ± 2.48	124.79 ± 6.37	9.13 ± 0.61
ACTPK1 OE24	18.42 ± 1.17	39.98 ± 0.26	105.77 ± 1.29	141.49 ± 4.39	10.28 ± 0.12
ACTPK1 OE33	19.08 ± 0.56	37.5 ± 1.36	95.05 ± 3.88	133.93 ± 12.95	10.3 ± 0.96
actpk1 ko12	12.22 ± 0.42	25.65 ± 0.44	67.6 ± 8.85	72.58 ± 9.65	6.53 ± 0.23
actpk1 ko14	14.10 ± 2.03	26.03 ± 0.54	59.89 ± 4.42	65.23 ± 5.89	6.42 ± 0.65
actpk1 ko19	12.59 ± 1.93	26.48 ± 0.7	62.38 ± 6.36	73.32 ± 9.63	5.98 ± 1.19

1071

1072

Figures and their legends:

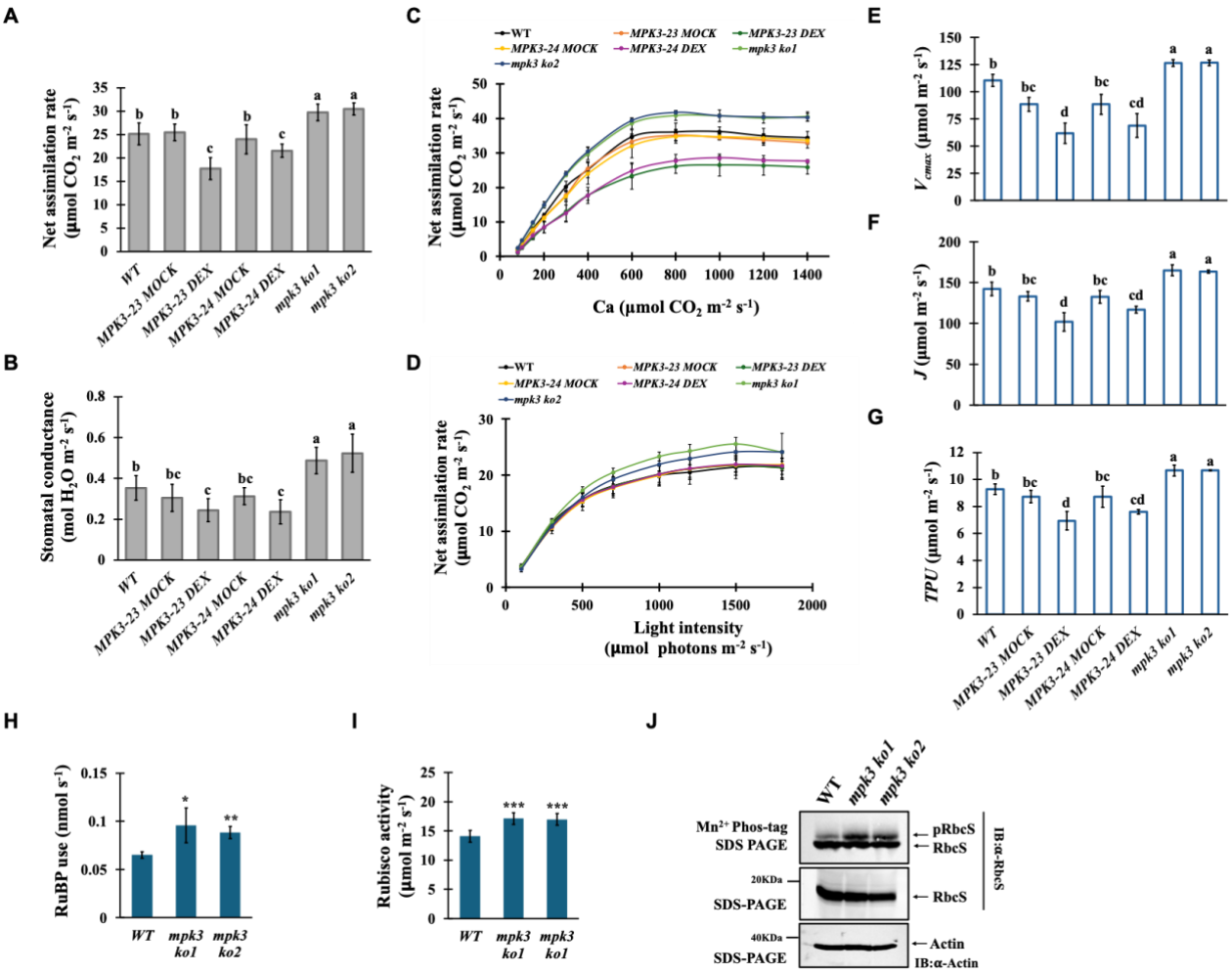

Fig. 1 MPK3 negatively regulates photosynthesis. **A)** Bar graph showing net assimilation rate in WT, *MPK3 OE* (*MPK3-23*, *MPK3-24*) and *mpk3 ko* (*mpk3 ko1*, *mpk3 ko2*) plants at ambient CO_2 (400 µmol mol^{-1}). **B)** Bar graph showing Stomatal conductance to water in WT, *MPK3 OE* (*MPK3-23*, *MPK3-24*) and *mpk3 ko* (*mpk3 ko1*, *mpk3 ko2*) plants at ambient CO_2 (400 µmol mol^{-1}). **C)** Quantification of net photosynthesis per unit area of WT, *MPK3 OE* (*MPK3-23*, *MPK3-24*) and *mpk3 ko* (*mpk3 ko1*, *mpk3 ko2*) plants in response to varying CO_2 concentration at 1500 µmol m^{-2} s^{-1} light intensity (*A/Ci* curve). Each value represents mean ± SD, where n = at least three data points from different plants. **D)** Quantification of net photosynthesis per unit area of WT, *MPK3 OE* (*MPK3-23*, *MPK3-24*) and *mpk3 ko* (*mpk3 ko1*, *mpk3 ko2*) plants in response to increasing PPFD at 400 µmol mol^{-1} CO_2 concentration (*A/Q* curve). Each value represents mean ± SD, where n = at least three data points from different plants. **E)** Bar graph showing maximum rate of carboxylation (*Vcmax*) in WT, *MPK3 OE* (*MPK3-23*, *MPK3-24*) and *mpk3 ko* (*mpk3 ko1*, *mpk3 ko2*) plants. **F)** Bar graph showing electron transport rate (*J*) in WT, *MPK3 OE* (*MPK3-23*, *MPK3-24*) and *mpk3 ko* (*mpk3 ko1*, *mpk3 ko2*) plants. **G)** Bar graph showing triose phosphate utilisation (*TPU*) in WT, *MPK3 OE* (*MPK3-23*, *MPK3-24*) and *mpk3 ko* (*mpk3 ko1*, *mpk3 ko2*) plants. Data represented in D), E) and F) are deduced by fitting *A/Ci* curve using FvcB model. MOCK, dimethyl sulfoxide treated (DMSO) plants; DEX, dexamethasone treated plants. 1 µM DMSO and DEX sprayed on *MPK3 OE* leaves, 24 h prior to taking measurements. All the measurements were taken from flag leaf at heading stage using LiCOR6800, between 8:00 am to 11:00 am. Different letters indicate statistical significance according to one-way ANOVA followed by post-hoc Tukey HSD calculation at $P < 0.05$. **H)** Bar graph showing RuBP use in WT, *MPK3 OE* (*MPK3-23*, *MPK3-24*) and

1096 *mpk3 ko* (*mpk3 ko1*, *mpk3 ko2*) plants. **I)** Bar graph showing Rubisco activity in WT, *MPK3 OE* (*MPK3-*
1097 *23*, *MPK3-24*) and *mpk3 ko* (*mpk3 ko1*, *mpk3 ko2*) plants**.** Values represent the mean ± SD (*n* = 3
1098 biological replicates). Asterix indicate statistical significance according to student ttest (*P*<0.05). **J)**
1099 Phos-tag gel western blots showing phosphorylated and non-phosphorylated RbcS content in WT and
1100 *mpk3 ko* lines. Blots were developed by α-RbcS antibody. Actin was used as endogenous control.

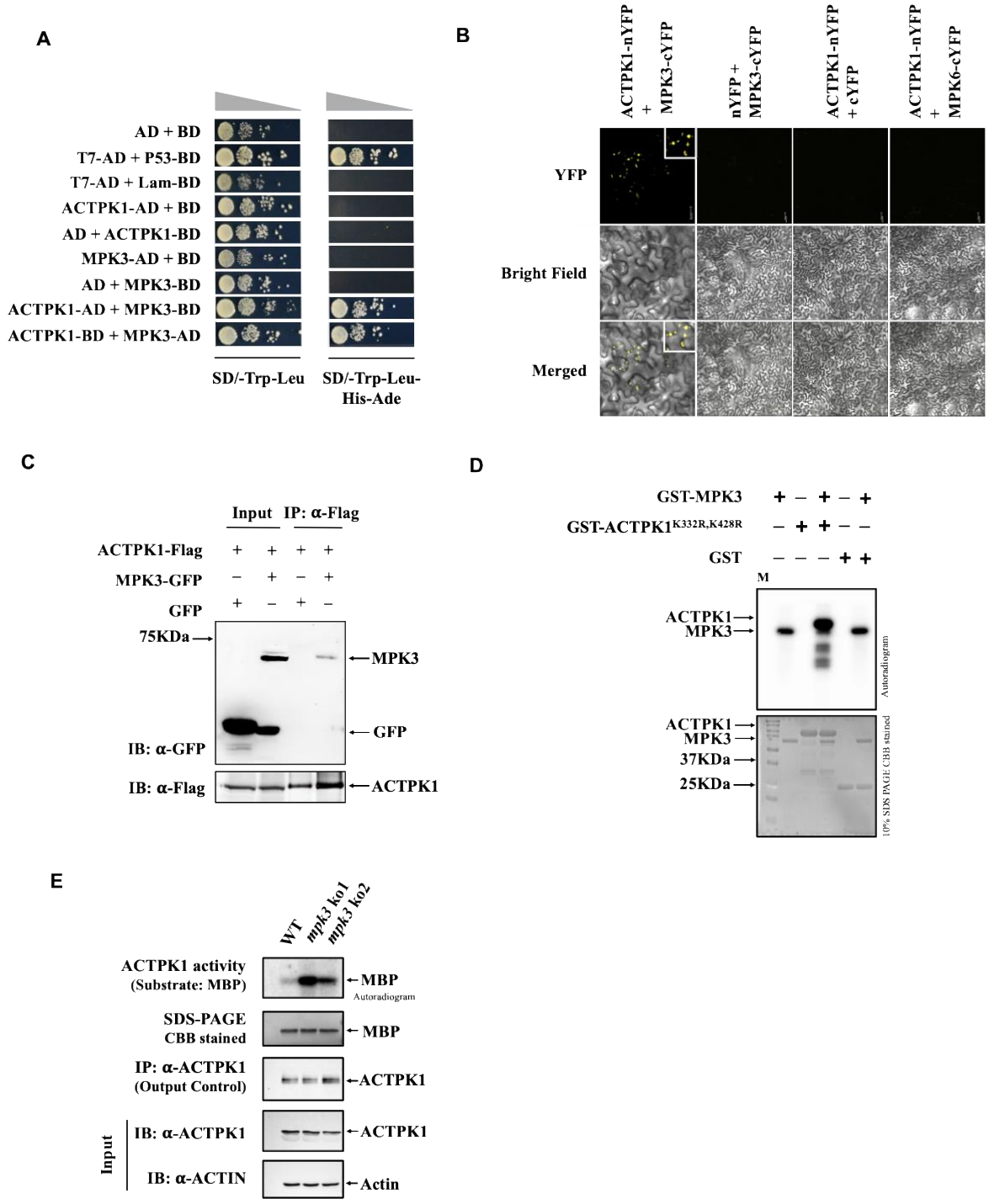

1101

1102 **Fig. 2 MPK3 physically interacts with and phosphorylates ACTPK1 to inhibit its activity. A)** MPK3
1103 interacts with ACTPK1 in yeast cells. Yeast cells were cultured on SD/-Trp-Leu and SD/-Trp-Leu-His-
1104 Ade media. AD, GAL4 activation domain; BD, GAL4 DNA-binding domain; SD, synthetic defined. **B)** BiFC
1105 assays showing that MPK3 interacts with ACTPK1 in *N. benthamiana*. ACTPK1-nYFP was co-

transformed with MPK3-cYFP in fully expanded leaves of *N. benthamiana*. The ACTPK1-nYFP/MPK6-cYFP and Empty-nYFP/MPK3-cYFP were used as negative controls. Inset on top right is the enlarged image of signal. Scale Bar, 25 μm. **C)** Interaction between MPK3 and ACTPK1 in the Co-IP assays. α-Flag beads were used to immunoprecipitate ACTPK1 protein. Gel blots were probed with α-GFP antibody. **D)** *In vitro* kinase assay showing phosphorylation of kinase dead GST-ACTPK1^{K332R,K428R} by GST-MPK3. CBB (Coomassie Brilliant Blue) stained 10% SDS page gel shows loaded proteins. **E)** IP-Kinase showing ACTPK1 immunoprecipitated from *mpk3 ko* enhances MBP phosphorylation. ACTPK1 was immunoprecipitated using α-ACTPK1 antibody.

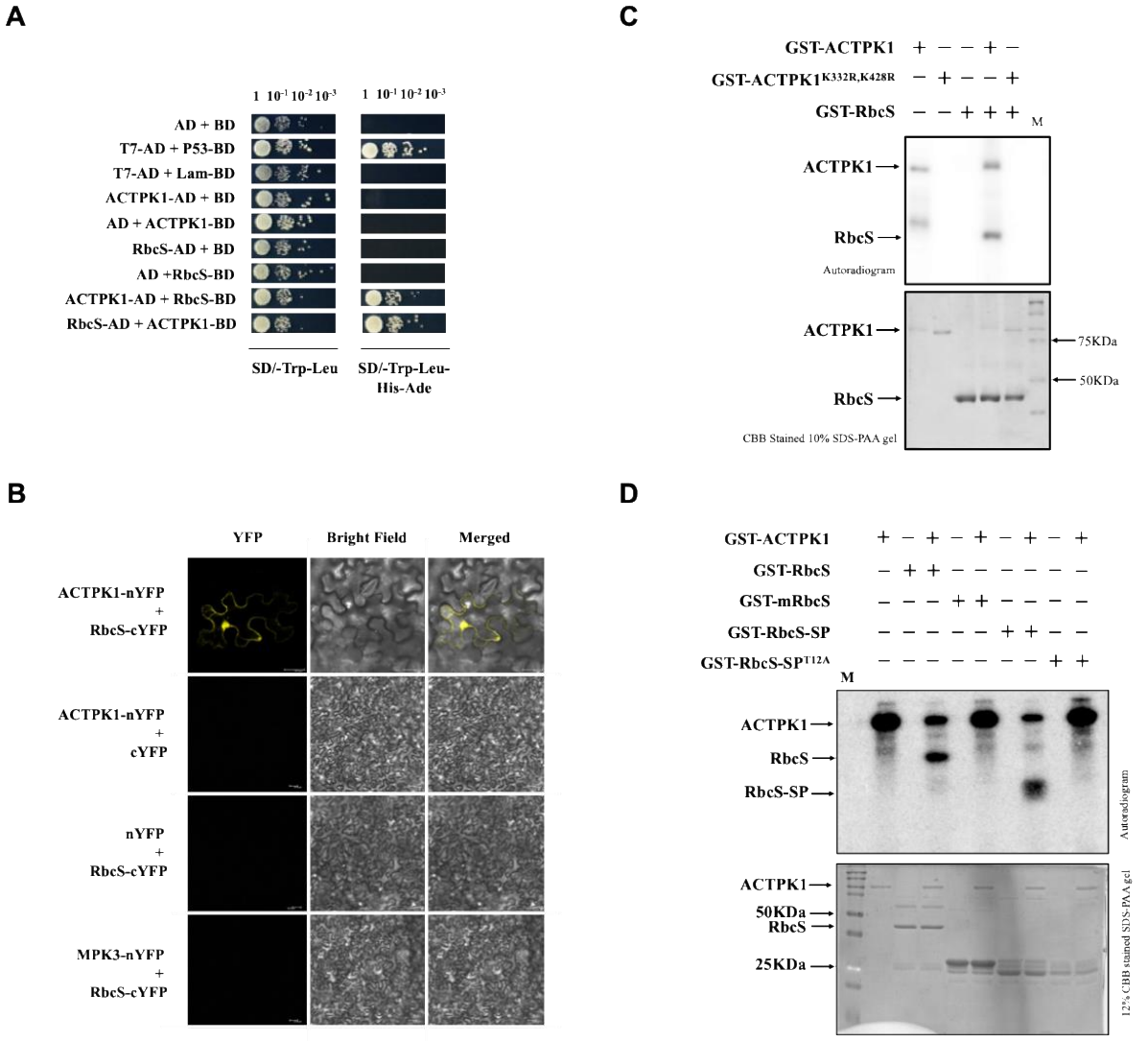

Fig. 3 ACTPK1 physically interacts with and phosphorylates RbcS within signal peptide. A) ACTPK1 interacts with RbcS in yeast cells. Yeast cells were cultured on SD/-Trp-Leu and SD/-Trp-Leu-His-Ade media. AD, GAL4 activation domain; BD, GAL4 DNA-binding domain; SD, synthetic defined. **B)** BiFC assays showing that ACTPK1 interacts with RbcS in *N. benthamiana* mesophyll cell. ACTPK1-nYFP was co-transformed with RbcS-cYFP in fully expanded leaves of *N. benthamiana*. The ACTPK1-nYFP/cYFP, nYFP/RbcS-cYFP and MPK3-nYFP/RbcS-cYFP were used as negative controls. Scale Bar, 25 μm. **C)** *In vitro* kinase assay showing phosphorylation of kinase dead GST-RbcS by GST-ACTPK1. CBB stained 10% SDS PAA gel shows loaded proteins. **D)** *In vitro* kinase assay showing ACTPK1 specifically phosphorylates Thr12 residue of RbcS**.** CBB stained 12% SDS PAA gel shows loaded proteins.

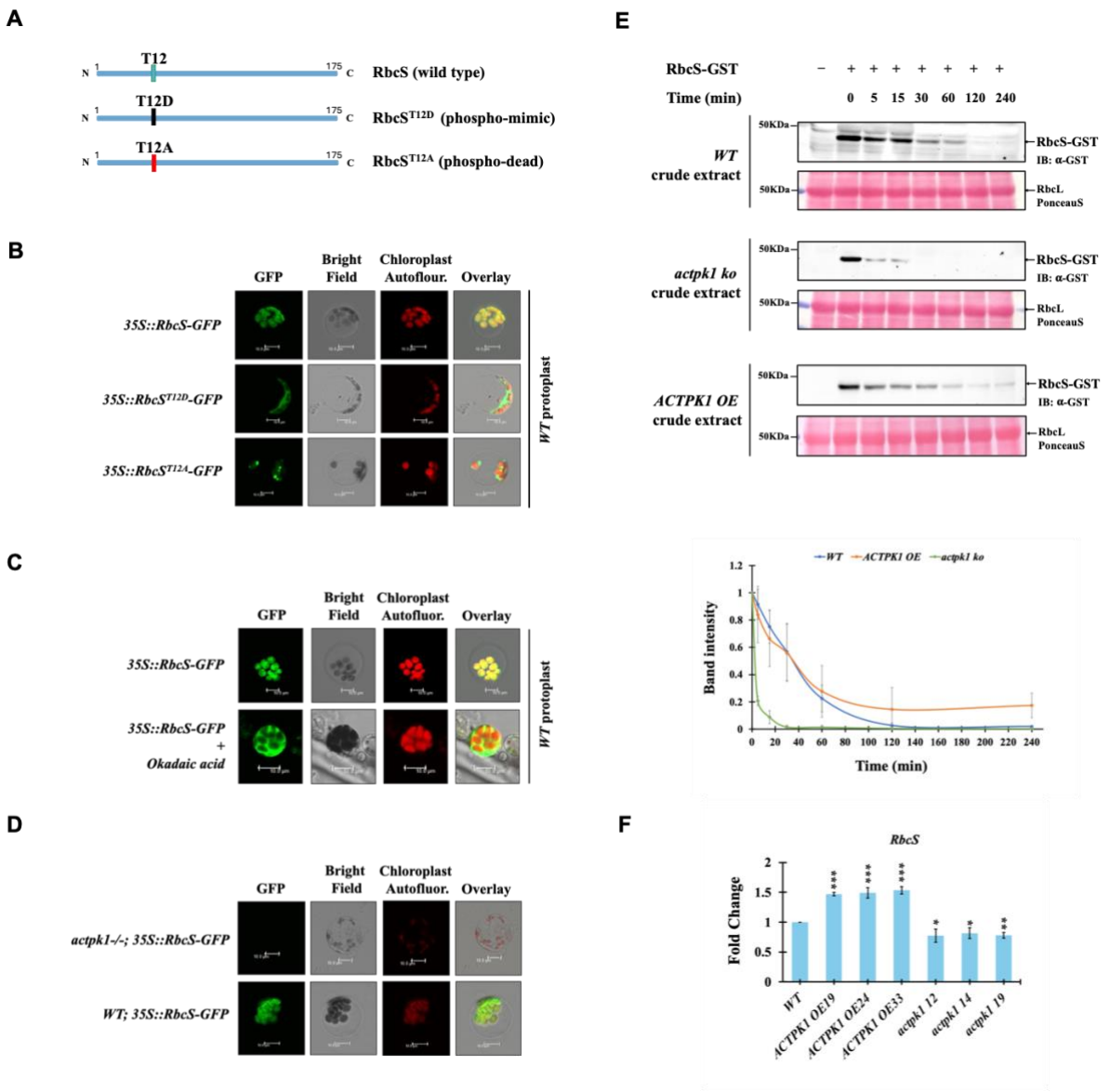

Fig. 4 ACTPK1 regulates stability and import of RbcS into the chloroplast. A) Pictorial representation of RbcS, RbcS^{T12D} (phosphor-mimic), RbcS^{T12A} (phosphor-dead) mutant constructs designed through site-directed mutagenesis. **B)** Localization of RbcS, RbcS^{T12D}, RbcS^{T12A} in protoplast isolated from WT rice seedlings. Scale Bar, 10 μm. **C)** Localization of RbcS in protoplast of WT rice seedlings treated with or without okadaic acid. 50nM okadaic acid for 30 min was used for treating WT protoplasts transfected with RbcS-GFP. Scale Bar, 10 μm. **D)** Localization of RbcS in the protoplasts of stable transgenic lines of WT and *actpk1 ko* overexpressing *RbcS* under the control of 35SCaMV promoter. Scale Bar, 10 μm. **E)** Western blots of cell-free degradation assays showing degradation of GST-RbcS when incubated with crude extract of WT (upper panel), *actpk1 ko* (middle panel) and *ACTPK1 OE* (lower panel). Ponceau stained (PonceauS) blot shows RbcL protein. Experiment was repeat thrice. **E)** Line graph depicting the band intensities as shown in (E). Band intensities were quantified using ImageJ software. **F)** Bar graph showing the RbcS transcript abundance in WT, *ACTPK1 OE* (*ACTPK1 OE19, ACTPK1 OE24 & ACTPK1 OE33*) and *actpk1 ko* (*actpk1 ko12, actpk1 ko14 & actpk1 ko19*). Actin7 and Ubq5 were used as internal control. Values represent the mean ± SD (n = 3 biological replicates). Asterix indicate statistical significance according to student ttest (P<0.05).

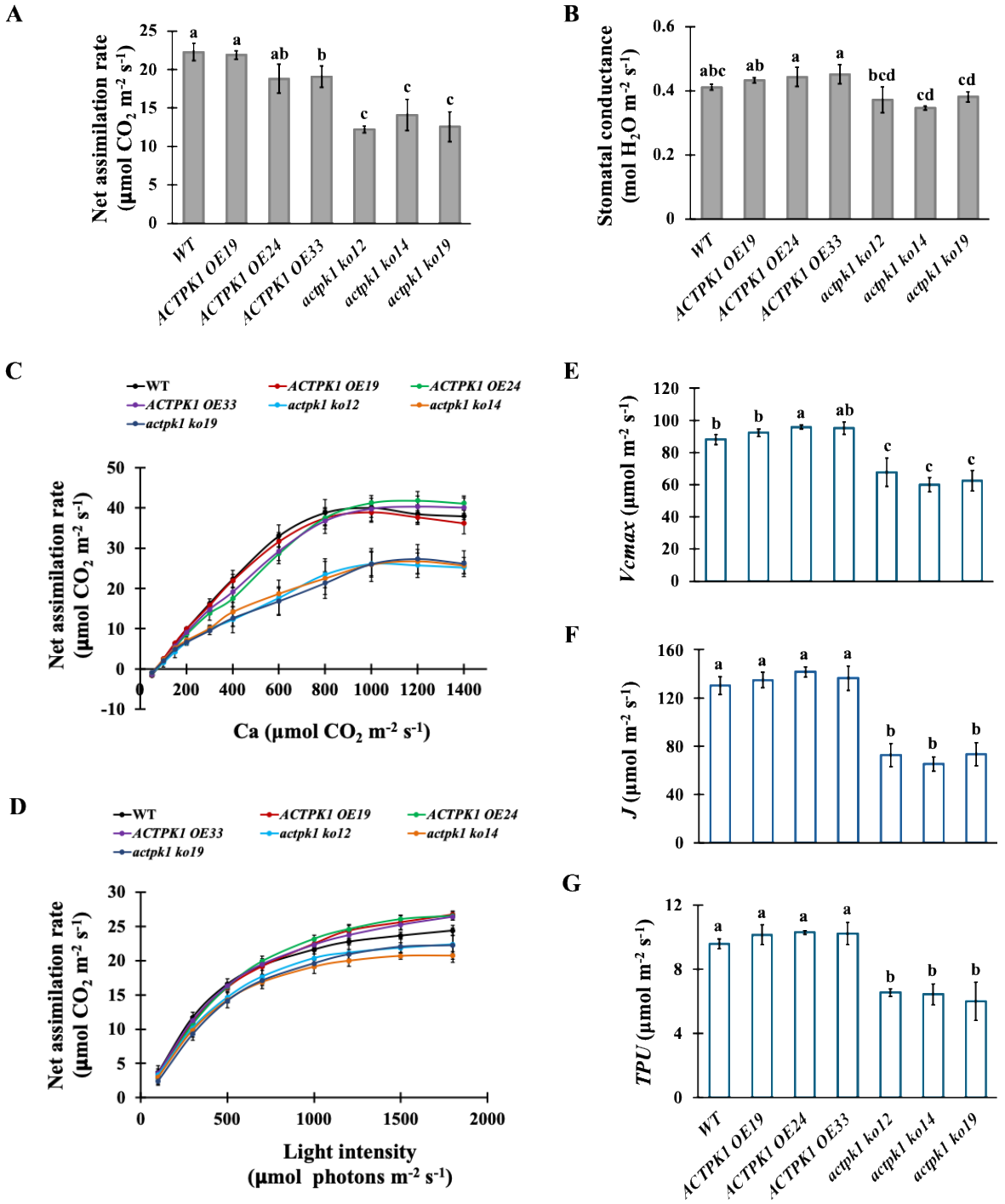

Fig. 5 ACTPK1 positively regulates photosynthesis in rice. A) Bar graph showing net assimilation rate in WT, *ACTPK1 OE* (*ACTPK1 OE19, ACTPK1 OE24 & ACTPK1 OE33*) and *actpk1 ko* (*actpk1 ko12, actpk1 ko14 & actpk1 ko19*) plants at ambient CO_2 (400 µmol mol^{-1}). **B)** Bar graph showing Stomatal conductance to water in WT, *ACTPK1 OE* (*ACTPK1 OE19, ACTPK1 OE24 & ACTPK1 OE33*) and *actpk1 ko* (*actpk1 ko12, actpk1 ko14 & actpk1 ko19*) plants at ambient CO_2 (400 µmol mol^{-1}). **C)** Quantification of net photosynthesis per unit area of WT, *ACTPK1 OE* (*ACTPK1 OE19, ACTPK1 OE24 & ACTPK1 OE33*) and *actpk1 ko* (*actpk1 ko12, actpk1 ko14 & actpk1 ko19*) plants in response to varying CO_2 concentration at 1500 µmol m^{-2} s^{-1} light intensity (*A/Ci* curve). Each value represents mean ± SD (n = at least three biological replicate). **D)** Quantification of net photosynthesis per unit area of WT, *ACTPK1 OE* (*ACTPK1 OE19, ACTPK1 OE24 & ACTPK1 OE33*) and *actpk1 ko* (*actpk1 ko12, actpk1 ko14 & actpk1*

ko19) plants in response to increasing PPFD at 400 µmol mol^{-1} CO_2 concentration (*A/Q* curve). Each value represents mean ± SD (n = at least three biological replicate). **E)** Bar graph showing maximum rate of carboxylation (*Vcmax*) in WT, *ACTPK1 OE* (*ACTPK1 OE19, ACTPK1 OE24 & ACTPK1 OE33*) and *actpk1 ko* (*actpk1 ko12, actpk1 ko14 & actpk1 ko19*) plants. **F)** Bar graph showing electron transport rate (*J*) in WT, *ACTPK1 OE* (*ACTPK1 OE19, ACTPK1 OE24 & ACTPK1 OE33*) and *actpk1 ko* (*actpk1 ko12, actpk1 ko14 & actpk1 ko19*) plants. **G)** Bar graph showing triose phosphate utilisation (*TPU*) in WT, *ACTPK1 OE* (*ACTPK1 OE19, ACTPK1 OE24 & ACTPK1 OE33*) and *actpk1 ko* (*actpk1 ko12, actpk1 ko14 & actpk1 ko19*) plants. Data represented in E), F) and G) are deduced by fitting *A/Ci* curve using FvcB model. All the measurements were taken from flag leaf at heading stage using LiCOR6800, between 8:00 am to 11:00 am. Different letters indicate statistical significance according to one-way ANOVA followed by post-hoc Tukey HSD calculation at $P < 0.05$.

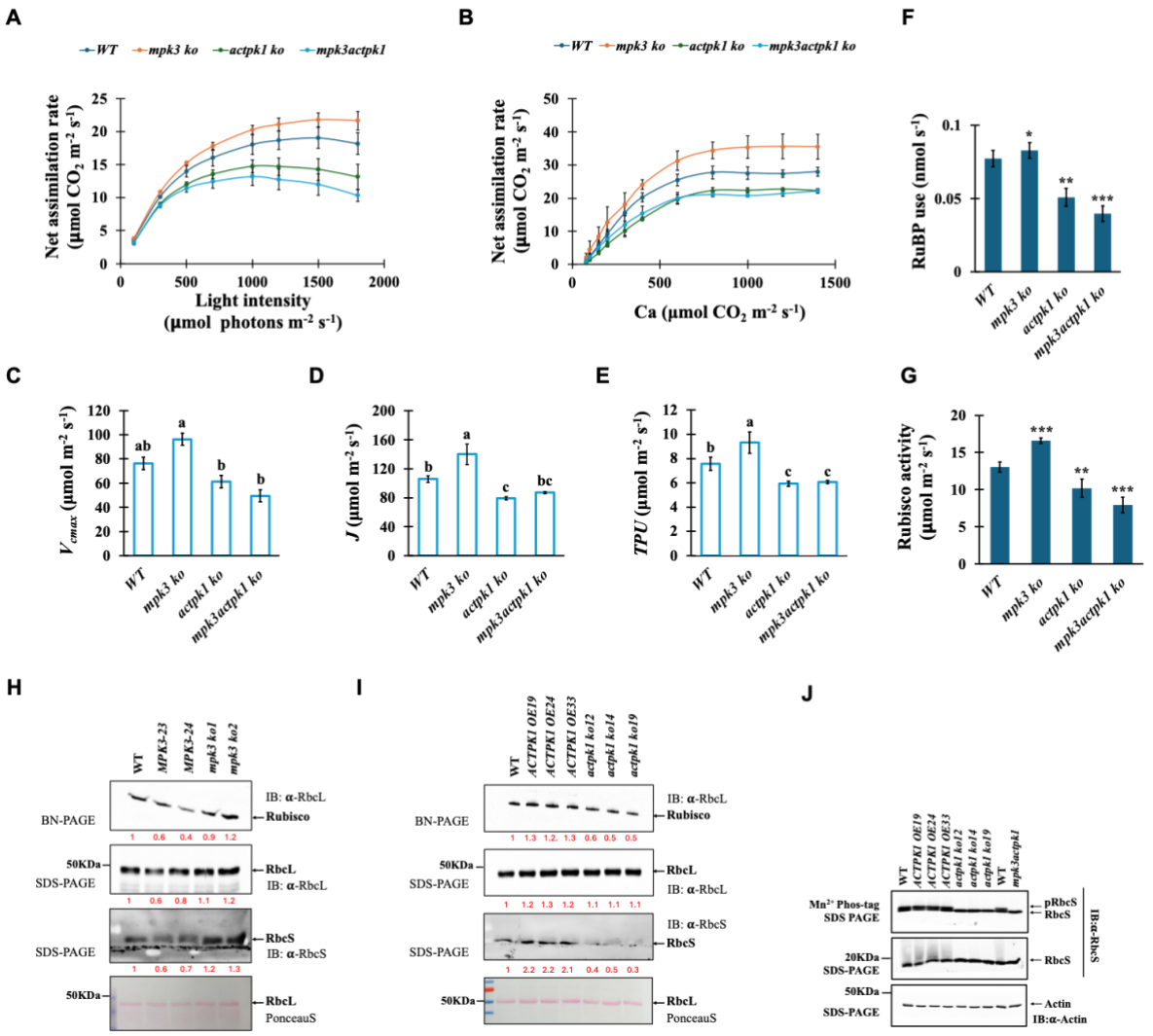

Fig. 6 ACTPK1 acts downstream of MPK3 to regulates photosynthesis in rice. A) Comparison of net photosynthesis per unit area of WT, *mpk3 ko*, *actpk1 ko* and *mpk3actpk1 ko* plants in response to varying CO_2 concentration at 1500 µmol m^{-2} s^{-1} light intensity (*A/Ci* curve). Each value represents mean ± SD, where n = at least three data points from different plants. **B)** Comparison of net photosynthesis per unit area of WT, *mpk3 ko*, *actpk1 ko* and *mpk3actpk1 ko* plants in response to increasing PPFD at 400 µmol mol^{-1} CO_2 concentration (*A/Q* curve). Each value represents mean ± SD, where n = at least three data points from different plants. **C)** Bar graph showing maximum rate of carboxylation (*Vcmax*) in WT, *mpk3 ko*, *actpk1 ko* and *mpk3actpk1 ko* plants. **D)** Bar graph showing electron transport rate (*J*) in of WT, *mpk3 ko*, *actpk1 ko* and *mpk3actpk1 ko* plants. **E)** Bar graph showing triose phosphate

1172 utilization (*TPU*) in of WT, *mpk3 ko*, *actpk1 ko* and *mpk3actpk1 ko* plants. Data represented in D), E)
1173 and F) are deduced by fitting *A/Ci* curve using FvcB model. All the measurements were taken from flag
1174 leaf at heading stage using LiCOR6800, between 8:00 am to 11:00 am. Different letters indicate
1175 statistical significance according to one-way ANOVA followed by post-hoc Tukey HSD calculation at P
1176 < 0.05. **F)** Bar graph showing RuBP use in in WT, *ACTPK1 OE* (*ACTPK1 OE19, ACTPK1 OE24 & ACTPK1*
1177 *OE33*) and *actpk1 ko* (*actpk1 ko12, actpk1 ko14 & actpk1 ko19*) and *mpk3actpk1 ko* lines. **G)** Bar graph
1178 showing Rubisco activity in WT, *ACTPK1 OE* (*ACTPK1 OE19, ACTPK1 OE24 & ACTPK1 OE33*) and *actpk1*
1179 *ko* (*actpk1 ko12, actpk1 ko14 & actpk1 ko19*) and *mpk3actpk1 ko* lines. Values represent the mean ±
1180 SD (n = 3 biological replicates). Asterix indicate statistical significance according to student ttest
1181 (P<0.05). **H)** Immunoblots showing Rubisco (upper panel), RbcL (middle panel) and RbcS (lower panel)
1182 content in WT, *MPK3 OE* (*MPK3-23 & MPK3-24*) and mpk3 ko (*mpk3 ko1 & mpk3 ko2*) plants. Blots
1183 were probed with α-RbcL antibody for Rubisco and RbcL and with α-RbcS antibody for RbcS content.
1184 **I)** Immunoblots showing Rubisco (upper panel), RbcL (middle panel) and RbcS (lower panel) content
1185 in in WT, *ACTPK1 OE* (*ACTPK1 OE19, ACTPK1 OE24 & ACTPK1 OE33*) and *actpk1 ko* (*actpk1 ko12, actpk1*
1186 *ko14 & actpk1 ko19*) plants. Blots were probed with α-RbcL antibody for Rubisco and RbcL and with
1187 α-RbcS antibody for RbcS content. Band intensities (written in red color) in (H) and (I) were quantified
1188 using ImageJ software. **J)** Phos-tag gel western blots showing phosphorylated and non-phosphorylated
1189 RbcS content in WT, *ACTPK1 OE* (*ACTPK1 OE19, ACTPK1 OE24 & ACTPK1 OE33*) and *actpk1 ko* (*actpk1*
1190 *ko12, actpk1 ko14 & actpk1 ko19*) and *mpk3actpk1 ko* (double mutant) lines. Blots were probed with
1191 α-RbcS antibody. Actin was used as endogenous control.

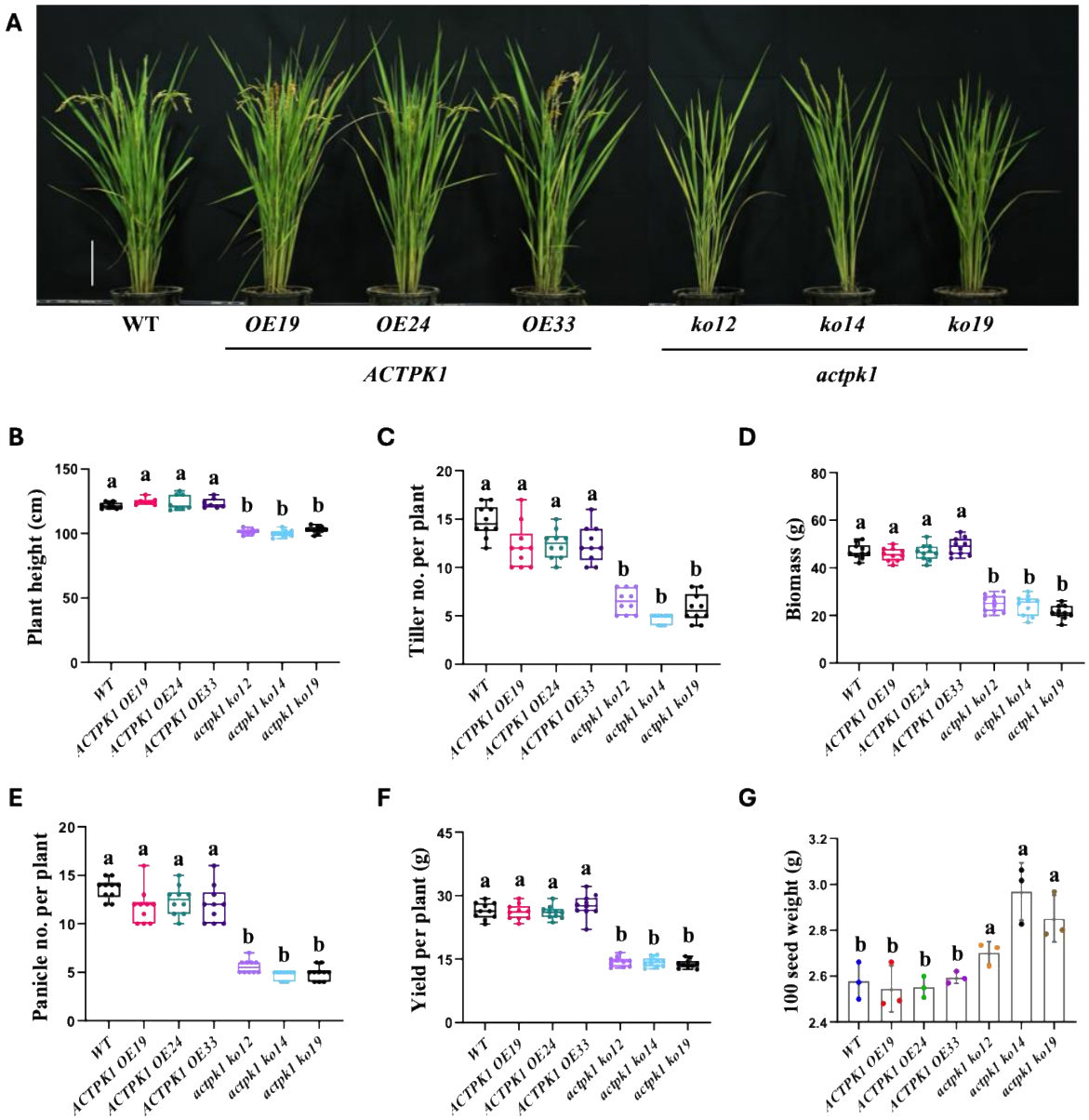

Fig. 7 ACTPK1 positively regulate plant biomass and yield. A) Representative image of WT, *ACTPK1 OE* (*ACTPK1 OE19, ACTPK1 OE24 & ACTPK1 OE33*) and *actpk1 ko* (*actpk1 ko12, actpk1 ko14 & actpk1 ko19*) plants. **B)-G)** Bar graph showing plant height **(B)**, tiller number per plant **(C)**, Biomass **(D)**, panicle number per plant **(E)**, yield per plant **(F)**, and 100 seed weight **(G)**, in WT, *ACTPK1 OE* (*ACTPK1 OE19, ACTPK1 OE24 & ACTPK1 OE33*) and *actpk1 ko* (*actpk1 ko12, actpk1 ko14 & actpk1 ko19*) plants. Values represent the mean ± SD (n = 10). Different letters indicate statistical significance according to one-way ANOVA followed by post-hoc Tukey HSD calculation at $P < 0.05$.

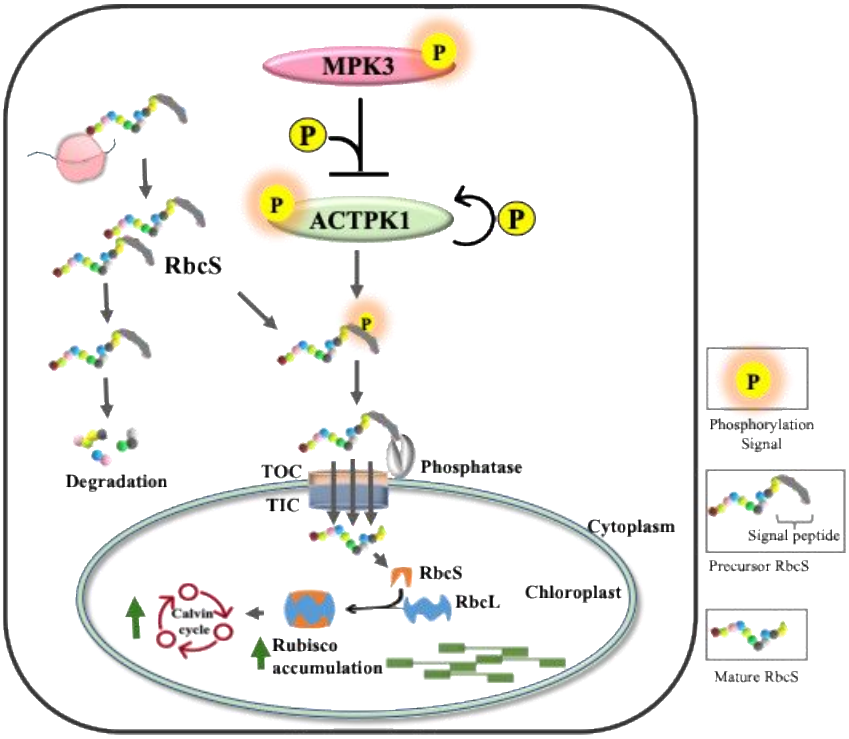

Fig. 8 A MAPK signaling module linking cytoplasmic signaling to Rubisco biogenesis. In this model, MPK3 phosphorylates and inhibits the Raf-like kinase ACTPK1. ACTPK1 directly phosphorylates the Rubisco small subunit precursor (RbcS) at Thr12 within its transit peptide, stabilizing the precursor and increasing its import competence into chloroplasts. Through this mechanism, the MPK3–ACTPK1–RbcS signaling cascade connects cytoplasmic kinase signaling with chloroplast protein biogenesis to fine-tune Rubisco accumulation and photosynthetic carbon fixation.